Modeling diurnal variation of surface $PM_{2.5}$ concentration over East China with WRF-Chem: Impacts from boundary layer mixing and anthropogenic emission

[1]Qiuyan Du, [1]Chun Zhao*, [1]Mingshuai Zhang, [1,2]Xue Dong, [1]Yu Chen, [3]Zhen Liu, [4]Zhiyuan Hu, [5]Qiang Zhang, [6]Yubin Li, [1]Renmin Yuan, [7]Shiguang Miao

[1]School of Earth and Space Sciences, University of Science and Technology of China, Hefei, China, 230026

[2]PowerChina Huadong Engineering Corporation Limited, Hangzhou, China

[3]School of Geosciences, University of Edinburgh, U.K.

[4]Key Laboratory for Semi-Arid Climate Change of the Ministry of Education, College of Atmospheric Sciences, Lanzhou University, Lanzhou, China

[5]Department of Earth System Science, Tsinghua University, Beijing, China

[6]School of Atmospheric Physics, Nanjing University of Information and Technology, Nanjing, China

[7]Institute of Urban Meteorology, Chinese Meteorology Administration, Beijing, China

Manuscript for submission to *Atmos. Chem. Phys.*

*Corresponding authors: Chun Zhao (chunzhao@ustc.edu.cn)

Key points:

1. Planetary boundary layer (PBL) mixing is the determinant factor in modeling the diurnal cycle of surface $PM_{2.5}$ concentrations over East China
2. Besides the PBL height, PBL mixing coefficient is also the key factor controlling the simulated diurnal cycle of surface $PM_{2.5}$ concentrations in WRF-Chem
3. The PBL mixing during the night over East China may be underestimated by WRF-Chem; Increase of PBL mixing during the night can significantly reduce the modeling biases of surface $PM_{2.5}$ concentrations and also the modeling sensitivity to the PBL configuration
4. The diurnal cycle and injection height of anthropogenic emission have impacts on simulating diurnal cycle of surface $PM_{2.5}$ concentrations but smaller than that from PBL mixing

Abstract

Diurnal variation of surface $PM_{2.5}$ concentration (diurnal $PM_{2.5}$) could dramatically affect aerosol radiative and healthy impact, and can also well reflect the physical and chemical mechanisms of air pollution formation and evolution. So far, diurnal $PM_{2.5}$ and its modeling capability over East China has not been investigated, and therefore, is examined in this study. Based on the observations, the normalized diurnal amplitude of surface $PM_{2.5}$ concentrations averaged over East China is the weakest (~1.2) in winter, and reaches ~1.5 in other seasons. The diurnal $PM_{2.5}$ shows the peak concentration during the night in spring and fall and during the daytime in summer. The simulated diurnal $PM_{2.5}$ with WRF-Chem and its contributions from multiple physical and chemical processes are examined in the four seasons. The simulated diurnal $PM_{2.5}$ with WRF-Chem is primarily controlled by planetary boundary layer (PBL) mixing and emission variations, and is significantly overestimated against the observation during the night. This modeling bias is likely primarily due to the inefficient PBL mixing of primary $PM_{2.5}$ during the night. The simulated diurnal $PM_{2.5}$ is sensitive to the PBL schemes and vertical layer configurations with WRF-Chem. Besides the PBL height, the PBL mixing coefficient is also found as the critical factor determining the PBL mixing of pollutants in WRF-Chem. With reasonable PBL height, the increase of lower limit of PBL mixing coefficient during the night can significantly reduce the modeling biases in diurnal $PM_{2.5}$ and also the mean concentrations, particularly at the major cities of East China. It can also reduce the modeling sensitivity to the PBL vertical layer configurations. The diurnal variation and injection height of anthropogenic emissions also play roles on simulating diurnal $PM_{2.5}$, but the impact is relatively smaller than that from the PBL mixing. This study underscores that more efforts are needed to improve the boundary mixing process of pollutants in models with observations of PBL structure and mixing fluxes in addition to PBL height, in order to simulate reasonably the diurnal $PM_{2.5}$ over East China. The diurnal variation and injection height of anthropogenic emissions are also necessary to be included to simulate the diurnal $PM_{2.5}$ over East China.

1. Introduction

The Yangtze River Delta (YRD) region of East China hosts the economic engine and a major portion of the Chinese population. During the past two decades, the rapid economic growth has resulted in significant elevated surface air pollutants over East China, especially particulate matter (PM), also called aerosols. Previous studies have indicated that exposure to the high concentrations of $PM_{2.5}$ (fine particulate matter with aerodynamic diameter less than 2.5 μm) can cause many health issues such as lung cancer (LC), ischemic heart disease(IHD), asthma, and nervous system breakdown (e.g., Seaton et al., 1995; Davidson et al., 2005; Pope III et al., 2006; Ho et al., 2018; Li et al., 2018; Liu T et al., 2018). It has become the fourth risk factor of deaths in China and 11.1% of all deaths are attributable to the ambient elevated concentrations of particulate matter (Gakidou et al., 2017). Besides the health impacts, atmospheric aerosols can also influence the radiative energy budget of the Earth's system through interacting with radiation, and serving as cloud condensation nuclei (CCN) and ice nuclei (IN) and hence modifying cloud microphysics and precipitation (e.g., Ackerman, 1977; Dickerson et al., 1997; Jacobson, 1998).

Many studies have investigated spatial and temporal variations of atmospheric aerosol over China in last decades. The $PM_{2.5}$ concentrations are higher in North China than in South China. The highest surface $PM_{2.5}$ concentrations appear in winter and the lowest in summer, and the highest and lowest surface $PM_{2.5}$ concentrations of a day often occur in the evening and afternoon, respectively (e.g., Gong et al., 2007; Fu et al., 2008; Hu et al., 2014; Wang ZF et al., 2014; Wang YG et al., 2014; Wang YJ et al., 2014; Geng et al., 2015; Xie et al., 2015; Zhang and Cao, 2015; Zhang H et al., 2015). Moreover, modeling analysis can help understand the chemical and physical processes affecting aerosol formation and evolution (e.g., Ying et al., 2009; Zhang et al., 2010; Liao et al., 2014; Wang YX et al., 2014; Wang YJ et al., 2014; Hu Z et al., 2016; Li et al., 2016; Yang et al., 2016; Hu J et al., 2016; Zhao et al., 2017). Yang et al. (2016) reproduced an increasing trend of winter $PM_{2.5}$ concentrations averaged over East China for 1985-2005 with the GEOS-Chem model, and found that the variations in anthropogenic emissions dominated the increase of winter surface $PM_{2.5}$ concentrations over East China and the variations in meteorological fields also played an important role in influencing the decadal increase in winter $PM_{2.5}$ concentrations over East China. Hu J. et al., (2016) investigated the spatial and temporal distribution of secondary organic aerosol (SOA) in China in 2013 with the WRF-CMAQ model and found that the

formation of SOA from biogenic emissions was significantly enhanced due to anthropogenic emissions.

Most of previous modeling studies focused on understanding the mechanisms driving PM variation on daily or seasonal scales or/and evaluating the simulation of daily and monthly mean PM concentrations over East China. Few studies evaluated the model performance in simulating diurnal cycle of surface PM concentrations and investigated the mechanisms underneath. However, the model capability of capturing diurnal cycle of surface PM concentrations is critical for revealing mechanisms of PM formation and evolution and may also affect simulating mean concentrations. Some studies also found that diurnal variation of surface PM concentrations can affect the daily average radiative forcing (e.g., Arola A et al., 2013; Kassianov et al., 2013; Kuang et al., 2015; Wang Z et al., 2015; Song et al., 2018). Based on the ground-based data collected in Hefei from 2007 to 2013, Wang Z et al. (2015) demonstrated that using daily averaged aerosol properties to retrieve the 24-h average direct aerosol radiative forcing can have positive biases of up to 7.5 W m^{-2} for the cases. Arola et al. (2013) found that the aerosol optical depth (AOD) diurnal cycles have significant impacts on the daily mean aerosol radiative forcing.

Previous studies have observed evident diurnal variations of surface PM over East China (e.g., Gong et al., 2007; Gu et al., 2010; Pathak et al., 2011; Feng et al., 2014; Hu et al., 2014; Huang et al., 2014; Ma et al., 2014; Zhang and Cao, 2015; Chen et al., 2016; Tao et al., 2016; Zhao et al., 2016; Chen et al., 2017; Jia et al., 2017; Guo H et al., 2017; Guo J et al., 2017;). Zhang and Cao (2015) used a long-term dataset of surface $PM_{2.5}$ concentrations measured at 190 cities of China, and found that the diurnal variation of the $PM_{2.5}$-to-CO ratio consistently displayed a pronounced peak during the afternoon, reflecting a significant contribution of secondary PM formation. Guo H et al. (2017) investigated the diurnal cycle of $PM_{2.5}$ in China with the observations obtained at 226 sites of China during the period of January of 2013 to December of 2015 and found the surface $PM_{2.5}$ concentrations reached the maximum in the morning over the YRD region.

Diurnal variation of surface PM concentrations can be controlled by many factors including emissions, chemical reactions, and meteorology (e.g., Wang et al., 2006; Huang et al., 2010; Wang et al., 2010; Menut et al., 2012; Qi et al., 2012; Quan et al., 2013; Tiwari et al., 2013; Li et al., 2014; Pal et al., 2014; Sun et al., 2015; Zhang and Cao, 2015; Roig et al., 2019; Xu et al., 2019). Wang et al. (2010) found that simulations with hourly emission inventory can reproduce the diurnal variation patterns and magnitude of AOD better than simulations with daily emission inventory. Xu et al. (2019) compared the diurnal cycles of

aerosol species between 2014 and 2016 observed by Aerodyne high-resolution aerosol mass spectrometer in Beijing and found that the increase of secondary inorganic nitrate, sulfate, and ammonium throughout the day in 2016 were mainly caused by the enhanced photochemical production. With the dataset of PBL height derived from the space-borne and ground-based lidar, Su et al. (2018) investigated the relationship between PBL height and surface PM concentrations across China and found nonlinearly negative responses of PM to PBL height evolution over polluted regions, especially when the PBL height is shallow and PM concentration is high.

Since very few studies evaluated the modeling performance of diurnal cycle of surface PM concentrations over East China and investigated the mechanisms underneath, this study investigates the WRF-Chem (Weather Research and Forecasting model coupled with Chemistry) simulation of diurnal variation of $PM_{2.5}$ over East China. WRF-Chem (Grell et al., 2005; Skamarock et al., 2008; Powers et al., 2017) is an online-coupled meteorology and chemistry model that simulates meteorological fields and air pollutant concentrations simultaneously. It has been widely used for studying the temporal and spatial variation of aerosols (e.g., Jiang et al., 2012; Zhou et al., 2014; Bei et al., 2016; Wang et al., 2016; Zhang et al., 2016; Zhong et al., 2016; Li P et al., 2017; Zhao et al., 2017; Zhou et al., 2017; Liu S et al., 2018; Ni et al., 2018) and their meteorological and climatic impacts over East China (e.g., Gong et al., 2007; Ding et al., 2013; Wu et al., 2013; Gao et al., 2014; Chen et al., 2014; Zhao et al., 2014; Zhang B et al., 2015; Zhang L et al., 2015; Huang et al., 2016; Liu et al., 2016; Petäjä et al., 2016; Zhao B et al., 2017). Most of the previous modeling studies with WRF-Chem over China investigated the influencing factors on spatial distribution and monthly or seasonal variation of PM. None of them focused on the performance of simulating diurnal variation of PM with WRF-Chem.

The study will examine the observed characteristics of diurnal variation of surface $PM_{2.5}$ concentrations over the YRD region of East China in four seasons of 2018. The WRF-Chem simulations are conducted for one month of each season over East China as shown in Fig 1a, and the simulated diurnal cycle of surface $PM_{2.5}$ concentrations will be evaluated through comparing with hourly observations of surface $PM_{2.5}$ concentrations released by the Ministry of Environmental Protection (MEP) of China for 190 stations over the YRD region of East China in 2018. The model is also used to investigate the mechanisms driving the diurnal cycle of surface $PM_{2.5}$. This study will focus on the impacts from meteorology and anthropogenic emissions on the diurnal variation of surface $PM_{2.5}$ concentrations. For meteorology, we will focus on the PBL mixing process that has been found largely

controlling the diurnal variation of surface pollutant concentrations (Liu M et al., 2018). For emissions, based on the findings of Wang et al. (2010) and Yang et al. (2019), the diurnal variation and injection height of emission will be investigated. The rest of the paper is organized as follows. The detailed introduction of WRF-Chem model and numerical experiments, anthropogenic emissions, and observations will be presented in Section 2. The examination of simulated diurnal variation of surface $PM_{2.5}$ concentrations and the impacts of PBL mixing and emission will be discussed in Section 3. The summary and discussion can be found in Section 4 and 5, respectively.

2. Methodology

2.1 Models and experiments

2.1.1 WRF-Chem

In this study, the version of WRF-Chem updated by University of Science and Technology of China (USTC version of WRF-Chem) is used. This USTC version of WRF-Chem includes some additional capabilities such as the diagnosis of radiative forcing of aerosol species, land surface coupled biogenic VOC (Volatile Organic Compounds) emission, aerosol-snow interaction compared with the publicly released version (Zhao et al., 2013a,b, 2014, 2016; Hu et al., 2019). Particularly, in order to understand the modeling mechanisms driving the diurnal variations of surface $PM_{2.5}$ concentrations over East China, this study updates the USTC version of WRF-Chem to include the diagnosis of contribution to surface $PM_{2.5}$ concentrations from individual process including transport, emission, dry and wet deposition, PBL mixing, and chemical production/loss through estimating the difference of surface $PM_{2.5}$ concentrations before and after individual process during the simulation. More specifically, the contribution of each process is estimated in the following formula:

$$\boldsymbol{CT_{P,S,T}} = \boldsymbol{C_{P,S,T}} - \boldsymbol{C_{P,S,T0}}$$

where $\boldsymbol{C_{P,S,T0}}$ and $\boldsymbol{C_{P,S,T}}$ represent the concentration of species *S* before (model time *T0*) and after (model time *T*), respectively, the process *P*. Therefore, $\boldsymbol{CT_{P,S,T}}$ represents the contribution of the process *P* to the change of concentration of species *S* during the time period (*T*-*T0*). For example, if *C0* and *C* represent the surface concentrations of $PM_{2.5}$ before (*T0*) and after (*T*), respectively, the PBL mixing, the contribution (*CT*) of PBL mixing to the change of surface concentrations of $PM_{2.5}$ during the time period (*T*-*T0*) can be estimated as (C-C0). The overall contribution during a specific time period (e.g., one day) can be obtained

through integrating $CT_{P,S,T}$ for this time period.

The Model for Simulating Aerosol Interactions and Chemistry (MOSAIC, Zaveri and Peter,1999; Zaveri et al.,2008) and the CBM-Z (carbon bond mechanism) photochemical mechanism (Zaveri and Peters, 1999) are used. The MOSAIC aerosol scheme includes physical and chemical processes of nucleation, condensation, coagulation, aqueous phase chemistry, and water uptake by aerosols. All major aerosol components including sulfate, nitrate, ammonium, black carbon (BC), organic matter (OM), sea salt, mineral dust, and other inorganics (OIN) are simulated in the model. OIN represents the unidentified aerosol species other than OM, BC, sulfate, ammonium, and nitrate in emissions if any, which are composed mostly of minerals in emissions in this study. Aerosol size distributions are represented by eight discrete size bins through the bin approach (Fast et al., 2006). Dry deposition of aerosol mass and number is simulated following the approach of Binkowski and Shankar (1995), which includes both particle diffusion and gravitational effects. Wet removal of aerosols by grid resolved stratiform clouds/precipitation includes in-cloud removal (rainout) and below-cloud removal (washout) by impaction and interception, following Easter et al. (2004) and Chapman et al. (2008). In this study, cloud-ice-borne aerosols are not explicitly treated in the model but the removal of aerosols by the droplet freezing process is considered. Convective transport and wet removal of aerosols by cumulus clouds follow Zhao et al. (2013a). Aerosol radiative feedback is coupled with the Rapid Radiative Transfer Model (RRTMG) (Mlawer et al., 1997; Iacono et al., 2000) for both SW and LW radiation as implemented by Zhao et al. (2011). The optical properties and direct radiative forcing of individual aerosol species in the atmosphere are diagnosed following the methodology described in Zhao et al. (2013b). A detailed description of the computation of aerosol optical properties in WRF-Chem can be found in Fast et al. (2006) and Barnard et al. (2010). Aerosol-cloud interactions were included in the model by Gustafson et al. (2007) for calculating the activation and re-suspension between dry aerosols and cloud droplets.

2.1.2 Numerical experiments

In this study, WRF-Chem is conducted with two nested domains (one-way nesting) in one month of each season of 2018 (i.e., January, April, July, October of 2018). The outer quasi-global domain with 360×145 grid cells (180°W~180°E,67.5°S~77.5°N) at the 1°×1° horizontal resolution is used to provide the chemical boundary to the inner domain with 112×105 grid cells (109.0°E~124.9°E, 24.0°N~38.9°N) at the horizontal resolution of 15 km

over East China covering the entire YRD region as shown in Figure 1a. More details about the quasi-global WRF-Chem simulation can be found in Zhao et al. (2013a) and Hu Z et al. (2016). To better resolve the PBL structure and mixing and examine the modeling sensitivity to vertical configuration within PBL, two experiments (CTL1 and CTL2, Table 1) are configured with 40 vertical layers but have different distributions (as shown Fig. 1b). One configuration (L1) has roughly 20 layers below 2 km above the ground, and the other has about 10 layers below 2 km (Fig. 1b). In both CTL1 and CTL2, MYNN2 PBL scheme (Nakanishi and Niino, 2006) is used. To demonstrate the modeling sensitivity to PBL parameterizations, the experiment CTL3 is conducted as the way similar to CTL2 but with the YSU PBL scheme (Hong et al., 2006). Since this study focuses on understanding the PBL mixing impact, the calculation of PBL mixing coefficient within the MYNN2 and YSU PBL schemes is briefly described here. In the local closure PBL scheme MYNN, the PBL mixing coefficient is calculated following Mellor et al. (1982):

$$K_{h,m} = lqS_{h,m}$$

where l is the mixing-length scale, S_h and S_m are stability functions, q is related to the turbulent kinetic energy (TKE) in the following formula:

$$\mathrm{q} = (2 * TKE)^{1/2}$$

In the non-local closure PBL scheme YSU, the momentum mixing coefficient K_m is formulated following Hong et al. (2006):

$$K_m = kw_s z(1 - \frac{z}{h})^p$$

where p is the profile shape exponent taken to be 2, k is the von-karman constant, z is the height from the surface and h is PBL height. For the eddy mixing coefficient for temperature and moisture K_h can be estimated from K_m with the relationship of the *Prandtl* number as in Noh et al. (2003):

$$\mathrm{Pr} = K_m/K_h$$

$$\mathrm{Pr} = 1 + (\mathrm{Pr}_0\text{-}1)\exp\left[\frac{\text{-}3(z\text{-}\varepsilon h)^2}{h^2}\right]$$

Two additional sensitivity experiments (EXP1 and EXP2, Table 1) are also conducted corresponding to the experiments CTL1 and CTL2, respectively, except that the PBL mixing coefficient is modified (see details in Section 3.2.2).

All these WRF-Chem experiments use the Morrison two-moment cloud microphysics (Morrison et al., 2009), Kain-Fritsch convective scheme (Kain et al., 2004), CLM land surface scheme, and RRTMG longwave and shortwave radiation schemes. The

meteorological initial and lateral boundary conditions are derived from the NCEP Final reanalysis data with 1°×1° resolution and 6-hour temporal resolution. The modeled u component and v component wind and atmospheric temperature are nudged towards the reanalysis data only to the layers above the PBL with nudging coefficients of 3×10^{-4} s^{-1} with a nudging timescale of 6-hour (Stauffer and Seaman, 1990; Seaman et al., 1995).

2.1.3 Emissions

Anthropogenic emissions for the outer quasi-global simulation are obtained from the Hemispheric Transport of Air Pollution version-2 (HTAPv2) at 0.1°×0.1° horizontal resolution and a monthly temporal resolution for year 2010 (Janssens-Maenhout et al., 2015), except that emissions over China within the domains are from the Multi-resolution Emission Inventory for China (MEIC) at 0.1°×0.1° horizontal resolution for 2015 (Li M et al., 2017a,b), which is also used for the inner domain simulation over East China. Figure 1a shows the spatial distributions of emissions of primary $PM_{2.5}$, NO_x, and SO_2 over East China. The default anthropogenic emission inventories assume no diurnal variation of emissions and that all emissions are near the surface (e.g., the first model layer). Since diurnal variation of emissions and injection height of power plant emissions may have impacts on diurnal variation of surface pollutants, the experiments discussed above apply the diurnal profiles of anthropogenic emissions from five individual sectors (i.e., agriculture, industry, transport, energy, and residential) following Olivier et al. (2003) and Wang et al. (2005) as shown in Fig. 1c and vertical distributions of anthropogenic power plant emissions following Wang et al. (2010) as shown in Table 2. Wang et al. (2010) derived the vertical profiles for East Asia based on the dataset of the U.S. and found that the profiles are comparable to those estimated in China and Japan (Woo et al., 2003; Wang et al., 2010). As shown in Fig. 1c, emissions from all sectors show peak values during the daytime, and the diurnal variations from agriculture, residential, and transportation are much stronger than those from industry and power plant. The emissions from power plant are distributed from the bottom to a height of ~900 m with more than 90% below 500 m. Both diurnal and vertical variation profiles of anthropogenic emissions are prescribed without temporal variability. Two sensitivity experiments, EXP1_E1 and EXP1_E2, are conducted as the way similar to EXP1 except that EXP1_E1 assumes no diurnal variation of anthropogenic emissions and EXP1_E2 assumes all power plant emissions are placed near the surface (i.e., the first model layer). Comparing EXP1 with EXP1_E1 and EXP1_E2 can examine the impact of diurnal variation and

injection height of anthropogenic emissions on diurnal cycle of surface $PM_{2.5}$, respectively. All these experiments are summarized in Table 1. Biomass burning emissions are obtained from the Fire Inventory from NCAR (FINN) with hourly temporal resolution and 1 km horizontal resolution (Wiedinmyer et al., 2011). The biomass burning emissions follow the diurnal variation provided by WRAP (2005) and the injection heights suggested by Dentener et al. (2006) from the Aerosol Comparison between Observations and Models (AeroCom) project. Sea-salt emission follows Zhao et al. (2013a), which includes correction of particles with radius less than 0.2 μm (Gong, 2003) and dependence of sea-salt emission on sea surface temperature (Jaeglé et al., 2011). The vertical dust fluxes are calculated with the GOCART dust emission scheme (Ginoux et al., 2001), and the emitted dust particles are distributed into the MOSAIC aerosol size bins following a theoretical expression based on the physics of scale-invariant fragmentation of brittle materials derived by Kok (2011). More details about the dust emission scheme coupled with MOSAIC aerosol scheme in WRF-Chem can be found in Zhao et al. (2010, 2013a).

2.2 Observations

The ground observations of hourly surface $PM_{2.5}$ mass concentrations in January, April, July, and October of 2018 are obtained from the website of the Ministry of Environmental Protection of China (MEP of China). Since this study focuses on the YRD region of East China, 190 stations over East China are selected for analysis. The locations of these 190 stations are shown in Fig. 1a within the black box (116.0°E~122.5°E,29.0°N~33.0°N). Besides regional average analysis, four cities (Fig. 1a) as the Center (Shanghai, 121.45°E and 31.21°N) and sub-Center (Nanjing, 118.78°E and 32.06°N; Hefei, 117.25°E and 31.85°N; Hangzhou, 120.08°E and 30.21°N) of the YRD city cluster are also selected for further analysis at urban areas.

3. Results

3.1 Modeling diurnal cycle of surface $PM_{2.5}$ concentration

In order to investigate the diurnal cycle of surface $PM_{2.5}$ concentrations, this study defines an index to better show the diurnal variation. The diurnal index (DI) is defined as the value of each hour divided by the minimum value within 24-hour on monthly average. The peak DI within 24-hour represents the amplitude of diurnal variation. Figure 2 shows the diurnal index of surface $PM_{2.5}$ concentrations within 24-hour averaged over the YRD region

of East China (as shown as the black box in Fig. 1a) for January, April, July, October of 2018 from the WRF-Chem experiments and observations. The experiment CTL1 uses the MYNN PBL scheme and finer boundary layer configuration (L1 in Fig. 1b). The simulation results and the observations are sampled 3-hourly at the observational sites as shown in Fig. 1a. On regional average, the observed variation of DI is the weakest in winter with the peak value around 1.2 among the four seasons. The observed DI reaches the maximum of 1.5 in autumn. In spring and autumn, the observed diurnal variation of DI are similar, showing the peak during the night, and reaching the minimum in the afternoon, which is consistent with previous findings with observations over East China (e.g., Zhang and Cao., 2015; Liu et al.,2016; Guo et al.,2017). In summer, different from other seasons, the observed diurnal variation of DI shows the single peak around 1.4 near the noon time. The CTL1 experiment can generally reproduce the peak during the night, however, the CTL1 simulation overestimates the observed peak DI in the two seasons, particularly in autumn. The experiment generally captures the seasonality of DI of surface $PM_{2.5}$ concentrations that is higher DI in spring and autumn and the weakest DI in winter, except that in summer the experiment significantly overestimates the DI during the night and produces opposite diurnal pattern with the minimum DI near the noon time. The spatial distributions of DI over East China are also generally consistent between observations and simulations and show similar seasonality (Figure S1 in the supporting material). The area with higher surface $PM_{2.5}$ concentrations generally has higher DI (Figure S2 in the supporting material), particularly from the simulation.

Therefore, the DI distributions at the four cities as the Center (Shanghai) and sub-Center (Nanjing, Hefei, Hangzhou) of the YRD city cluster in East China (as shown in Fig. 1a) are further analyzed. Figure 3 shows the diurnal index of surface $PM_{2.5}$ concentrations within 24-hour averaged over the four cities for January, April, July, October of 2018 from the WRF-Chem experiments and observations. The observed diurnal variation of DI in these four cities are consistent with that on regional average of East China. The diurnal variation of DI are more evident in the two inland cities (Hefei and Nanjing) than the two coastal cities (Hangzhou and Shanghai). Consistent with the results based on regional average, the CTL1 experiment can generally capture the diurnal variation of DI of surface $PM_{2.5}$ in the four cities, but overestimates the DI in the night, particularly in spring and autumn. In summer, again, the CTL1 significantly overestimates the DI during the night and produces the opposite diurnal pattern compared to observations. In general, the CTL1 produces even higher DI during the night in the four cities than regional average, which results in larger diurnal

amplitudes in the four cities than regional average. The CTL1 can generally simulate stronger diurnal variation in the two inland cities than in the two coastal cities.

The analysis above for both regional average and city average indicates that the CTL1 simulation has high positive biases of DI during the night. In order to understand the modeling biases and the mechanisms driving the simulated diurnal variations of surface $PM_{2.5}$ concentrations over East China, the contribution to diurnal variation of surface $PM_{2.5}$ concentrations from individual process including transport, emission, dry and wet deposition, mixing, and chemical production/loss is estimated. The contribution is calculated as the difference of surface $PM_{2.5}$ concentrations before and after individual process during the simulation. Figure 4 shows the contribution of individual process to the variation of surface $PM_{2.5}$ concentrations every 3-hour in Hefei from the WRF-Chem experiments averaged for January, April, July, and October of 2018. The 3-hourly tendency (the difference between the current time and the time 3-hour earlier) of surface $PM_{2.5}$ concentrations is also shown. The contributions and tendencies are divided by monthly mean surface $PM_{2.5}$ concentrations for each month. The results for the other three cities (Nanjing, Hangzhou, Shanghai) are similar to that of Hefei and are shown in the supporting material (Figure S3a-c). Process contribution analysis is verified by comparing the variations of surface $PM_{2.5}$ concentrations with the sum of the contributions from each individual process. As shown in Figure S4, the sum contributions of all processes are consistent with the variations in surface $PM_{2.5}$ concentrations following the principle of mass balance.

In Fig. 4, positive value denotes relative increase of surface $PM_{2.5}$ concentrations and negative value denotes relative decrease. From the CTL1 experiment, the contributions from emission and chemistry are positive through the day, while the contributions from transport, PBL mixing, wet and dry deposition are negative through the day. The CTL1 simulates the largest variation of tendency in summer and the smallest variation in winter. The tendencies are negative from the morning to the afternoon, resulting the simulated minimum surface $PM_{2.5}$ concentrations in the afternoon in all seasons, which is consistent with the result shown in Fig. 3. It is evident that emission, PBL mixing, and transport are the three main processes controlling the diurnal variation of surface $PM_{2.5}$ concentrations, and emission and PBL mixing are the dominant two. Emission increases the surface $PM_{2.5}$ concentrations and reaches the maximum near the noon time, while PBL mixing reduces the surface $PM_{2.5}$ concentrations and also reaches the maximum reduction near the noon time. The combined effect of emission and PBL mixing is reflected as the overall tendency. Therefore, PBL mixing is the determinant process leading to the simulated minimum DI near the noon time

and higher DI during the night. To further demonstrate the contribution of each $PM_{2.5}$ composition to the diurnal variation of surface $PM_{2.5}$ concentrations, Figure 5 shows the diurnal variation of surface concentration of each $PM_{2.5}$ composition in Hefei from the WRF-Chem experiments averaged for January, April, July, and October of 2018. The diurnal variations of surface concentrations of OM, BC, and OIN are larger than other components of $PM_{2.5}$, showing evident higher concentrations during the night and minimum near the noon time in all seasons except winter. The sum of OM and OIN contribute to more than half of surface $PM_{2.5}$ concentrations. Therefore, it suggests that the PBL mixing of the primary $PM_{2.5}$ determines the simulated diurnal variation of surface $PM_{2.5}$ concentrations. The results for the other three cities (Nanjing, Hangzhou, Shanghai) are similar to that of Hefei and are shown in the supporting material (Figure S5a-c).

In order to understand the possible reasons for this modeling biases, some basic meteorological fields are evaluated with available observations. Since the modeled winds at the layers above the PBL are nudged towards the reanalysis data, the large-scale circulation can be well simulated. The winds at 850 hPa for each season are compared with the NCEP Final reanalysis dataset (FNL) and ERA5 reanalysis dataset (https://rda.ucar.edu/datasets/ds630.0/, last access: 28 December 2019) (Fig. S6 in the supporting material). The simulated wind circulation is highly correlated with the two reanalysis datasets with the spatial correlation coefficients of 0.9-0.97 over East China. The simulated temperature at 2m is also evaluated with the available observations by the China Meteorological Administration (CMA) at the stations of East China (Fig. S7 and Fig. S8 in the supporting material). The model captures the diurnal variation of near-surface temperature very well over East China. For near surface winds, although the model generally overestimates the observed values by less than 10%, the simulated diurnal variation is generally consistent with the observations over East China (Fig. S9 and Fig. S10 in the supporting material). As the evaluation shows, the basic meteorological fields are generally simulated reasonably. The characteristics associated with the PBL mixing are further investigated below.

3.2 Sensitivity to PBL mixing

3.2.1 Sensitivity to the PBL configuration

As discussed above, the PBL mixing is very important for modeling diurnal variation of surface $PM_{2.5}$ concentrations, and it may be affected by PBL parameterizations and vertical layer configurations within the PBL. Therefore, two experiments, CTL2 and CTL3, are

conducted to examine the sensitivity of simulated diurnal variation of surface $PM_{2.5}$ concentrations to different PBL configurations. The CTL2 uses the MYNN PBL scheme as the CTL1 but is configured with different vertical layer distribution (L2) as shown in Fig. 1b, in which less vertical layers are put within the PBL as described in Section 2.2. The CTL3 uses the YSU PBL scheme and is configured with the L2 vertical layer distribution as the CTL2. As shown in Fig. 2, on regional average, the CTL2 and CTL3 generally simulate similar diurnal and seasonal patterns as that by the CTL1 with the minimum DI near the noon time and the peak DI during the night. The CTL2 simulates lower DI than the CTL1 during the night in all seasons. This indicates that the model with finer vertical resolution within the PBL, which is supposed to better resolve the PBL structure, produces higher positive biases of DI. The CTL3 simulates similar diurnal variation of DI as the CTL2 but overestimate the DI during the night to some extent, particularly in summer, which indicates the model with the YSU PBL scheme produces higher positive biases of DI during the night compared to the one with the MYNN PBL scheme. In the four cities as shown in Fig. 3, the CTL2 and CTL3 also simulate similar diurnal and seasonal patterns as that by the CTL1. It is also interesting to note that the difference of DI between CTL2 and CTL1 is larger than that between CTL3 and CTL2, which indicate that the modeling sensitivity of DI to the vertical layer configurations within the PBL is even greater than that to the PBL schemes. Overall, all these three WRF-Chem experiments produce similar positive biases of DI during the night compared to the observations in all seasons over the YRD region of East China, particularly in cities. This is consistent with previous findings about the simulated positive biases of diurnal variation of surface $PM_{2.5}$ concentrations over East China (e.g., Liu M et al., 2018). Liu M et al. (2018) found that the air quality model (WRF-CMAQ v5.0.1) also overestimated the surface concentrations of $PM_{2.5}$ during the nighttime in October-December, 2013. They speculated that the overestimation is due to the weak PBL mixing in the nighttime, and claimed that the newer version of CMAQ v5.1 driven by WRF v3.7 revised the PBL mixing scheme (ACM2) and might reduce the nighttime biases. To verify this, two experiments are conducted using the ACM2 PBL scheme with WRF-Chem v3.5 and WRF-Chem v4.0, respectively, over East China for October of 2018. The results showed that the PBL mixing of ACM2 scheme is enhanced in v4.0 compared to v3.5 especially during the night, and the simulated nighttime surface $PM_{2.5}$ concentrations are reduced to some extent in v4.0 compared to v3.5 (not shown). However, the simulation still significantly overestimates the surface $PM_{2.5}$ concentrations during the night. Therefore, the changes of PBL schemes and

vertical configurations within the PBL can affect the simulated DI but cannot improve the simulations to reproduce the observations.

In order to better understand the modeling sensitivity of DI to the PBL configuration, Fig. 4 and 5 also show the simulated results for the city of Hefei from the CTL2 and CTL3. Similar as CTL1, the results from CTL2 and CTL3 also show that emission, PBL mixing, and transport are the three main processes controlling the diurnal variation of surface $PM_{2.5}$ concentrations, and emission and PBL mixing are the dominant two (Fig. 4). Since the number of vertical layer within the PBL in CTL2 and CTL3 is much less than that in CTL1, the thickness of first model layer in CTL2 and CTL3 is about a factor 2 of that in CTL1. With the same emission flux, CTL2 and CTL3 simulate much smaller contributions from emission to the surface $PM_{2.5}$ concentrations than does CTL1. Correspondingly, the contributions from PBL mixing to the surface $PM_{2.5}$ concentrations in CTL2 and CTL3 are also lower than that in CTL1. The combined effect of emission and PBL mixing results in weaker diurnal variation of surface $PM_{2.5}$ concentrations in CTL2 and CTL3 than that in CTL1, as shown by the diurnal variation of overall tendency of surface $PM_{2.5}$ concentrations. CTL3 with the YSU PBL scheme simulates stronger diurnal variation of surface $PM_{2.5}$ concentrations than does the CTL2 with the MYNN PBL scheme, primarily due to its larger diurnal variation of PBL mixing. With less contribution from emission to the surface $PM_{2.5}$ concentrations, CTL2 and CTL3 simulate less primary $PM_{2.5}$ (OIN, OM, BC) than does CTL1 (Fig. 5), particularly during the night when the PBL mixing is weak. This leads to the weaker diurnal variation of total surface $PM_{2.5}$ concentrations in CTL2 and CTL3 as discussed above. The higher DI during the night in CTL3 than CTL2 can also be explained by the higher primary $PM_{2.5}$ during the night due to weaker PBL mixing.

3.2.2 Sensitivity to the PBL mixing coefficient

The results discussed above suggest that, the WRF-Chem simulated diurnal variation of surface $PM_{2.5}$ concentrations over East China is largely controlled by the PBL mixing process, and is sensitive to the PBL scheme and vertical layer configuration within the PBL. However, the increase of number of vertical layers within the PBL and use of different PBL schemes cannot reduce the modeling biases in diurnal variation of surface $PM_{2.5}$ concentrations. Many previous studies investigated the PBL mixing of pollutants through establishing the relationship between surface pollutant concentration and PBL height. However, it is noteworthy that in most atmospheric models, the mixing of pollutants within the PBL is treated either as full mixing within the PBL heights (i.e., uniformly distributed within the

PBL heights) or as calculated based on the mixing coefficient diagnosed from the PBL scheme. The former method represents the strongest PBL mixing and the surface concentrations can be largely influenced by the PBL heights. The latter one means that the pollutant mixing does not depend explicitly on PBL heights, although the PBL heights still reflects the boundary mixing strength.

In WRF-Chem, the PBL mixing of pollutants is treated with the second approach. In order to further examine the simulated PBL mixing process in this study, Figure 6 shows the diurnal variation of PBL heights and PBL mixing coefficients below PBL heights in Hefei in January, April, July, and October of 2018 from the WRF-Chem experiments CTL1, CTL2, and CTL3. The black line represents the PBL heights while the contour shading represents the PBL mixing coefficients within the PBL heights. First of all, the PBL heights simulated from the three experiments all show evident diurnal variation with the maximum in the daytime and the minimum during the night. The simulated PBL heights from CTL1 and CTL2 with the same PBL scheme (MYNN) show very similar diurnal pattern, indicating the vertical layer configuration has small impact on modeling PBL heights. Both experiments simulate the largest diurnal variation of PBL heights in summer with a changing factor of ~10 from ~2 km in the afternoon to ~200 m in the early morning, and the smallest diurnal variation of PBL heights in winter with a changing factor of 2 from ~700 m in the afternoon to ~350 m in the early morning. The CTL3 simulation with the YSU PBL scheme shows similar diurnal variation of PBL heights as those from the CTL1 and CTL2 simulations. The CTL3 simulates similar PBL heights during the daytime but lower values during the night, particularly in October. The simulated PBL heights are evaluated with the long-term averaged PBL heights, primarily for 8 am and 8 pm local time, derived from the air sounding observations available at the four stations of East China as reported in Guo et al. (2016) (Fig. S11 in the supporting material). In general, throughout the four seasons, the CTL3 with the YSU scheme simulates reasonable PBL heights in the early morning and night, while the CTL1 and CTL2 with the MYNN scheme overestimate the PBL heights compared to the derived values. The comparison between simulations and observations (Fig. 2 and 3) suggests the positive modeling biases of DI during the night may be partly due to the underestimation of the PBL mixing during the night, which cannot be explained by the positive modeling biases of PBL heights during the night.

It should be noted that the PBL mixing coefficients within the PBL in all the three experiments also exhibit evident diurnal variation with a changing factor of ~1000 and ~50 in summer and winter, respectively, which is much larger than that of the PBL height in all

seasons. More WRF experiments with different PBL schemes are conducted and all show similar results that the diurnal variation of PBL mixing coefficients is much stronger than that of PBL heights (not shown). With relatively large values of PBL mixing coefficient during the daytime, the emitted pollutants can be mixed up roughly reaching the layer of PBL heights. Therefore, the PBL height is very critical for determining the surface pollutant mixing strength during the daytime. However, weak PBL mixing coefficient during the night results in that the emitted $PM_{2.5}$ and its precursors will stay near the surface (i.e., within the first layer of model) during the night and cannot be mixed up reaching the PBL height (Fig. S12 in the supporting material). This leads to the large difference of DI between CTL1 and CTL2 with different thicknesses of first model layer during the night although they simulate similar PBL heights. Another example in autumn, the PBL heights during the night are lower in CTL3 than in CTL1, while the DI during the night are higher in CTL1 than in CTL3 (Fig. 3) due to the weak PBL mixing coefficients during the night that cannot mix the pollutants up to the PBL height. This further demonstrates that the WRF-Chem simulated diurnal variation of surface $PM_{2.5}$ concentration is not explicitly controlled by the PBL height instead by the PBL mixing coefficient. In fact, in WRF-Chem, there is an existing empirical parameterization to enhance the PBL mixing of pollutants in urban area based on the strength of anthropogenic emissions. However, it is only applied to gas pollutants if the MOSAIC aerosol scheme is selected as this study. It also tends to enhance the mixing up to half number of model vertical layers, which is beyond the PBL in most cases during the night. In this study, in order to examine the sensitivity of simulated DI to the PBL mixing coefficient, the sensitivity experiments, EXP1 and EXP2, are conducted corresponding to CTL1 and CTL2, respectively, through setting the lower limit of PBL mixing coefficient from 0.1 m^2/s (default in the publically released version of WRF-Chem) to 5 m^2/s within the PBL, which is applied to both gas and aerosol pollutants.

Figure 7 shows the simulated PBL height and mixing coefficients from the two sensitivity experiments, EXP1 and EXP2, in January, April, July, and October of 2018 in Hefei. It shows that the PBL mixing coefficient increases during the night within the PBL compared to the results shown in Fig. 6, while the values during the daytime remain almost the same. The difference of simulated surface $PM_{2.5}$ between CTL1 and EXP1 is relatively small during the daytime, but significant during the night, which is due to that EXP1 can mix up the surface $PM_{2.5}$ to the PBL heights during the night (Fig. S12). It is noteworthy that the lower limit parameter of 5 m^2/s is entirely empirical. It is selected to represent the moderate mixing strength between the full PBL mixing and no PBL mixing. A few other values such as

570 1 m^2/s and 10 m^2/s are also tested. The results do not change the conclusion found in this
571 study and therefore are not shown.
572 The change of PBL mixing coefficient during the night can significantly affect the
573 diurnal variation of PBL mixing. Figure 8 shows the contribution of individual process to the
574 variation of surface $PM_{2.5}$ concentrations every 3-hour in Hefei simulated by EXP1 and
575 EXP2 averaged for January, April, July, and October of 2018. The 3-hourly tendency of
576 surface $PM_{2.5}$ concentrations is also shown. Same as Fig. 4, the contributions and tendencies
577 are divided by monthly mean surface $PM_{2.5}$ concentrations for each month. The results for the
578 other three cities (Nanjing, Hangzhou, Shanghai) are similar to that of Hefei and are shown in
579 the supporting material (Figure S13a-c). Compared to the results from CTL1 and CTL2
580 shown in Fig. 4, it is evident that the diurnal variation of tendency of surface $PM_{2.5}$
581 concentrations is significantly reduced in all seasons. This is mainly resulted from the
582 significantly increased diurnal variation of PBL mixing contribution. Specifically, the PBL
583 mixing contribution during the night is increased. Figure 9 shows the diurnal variation of
584 surface concentration of each $PM_{2.5}$ composition in Hefei simulated by the EXP1 and EXP2
585 averaged for January, April, July, and October of 2018. The diurnal variations of surface
586 concentrations of OM, BC, and OIN are significantly reduced primarily due to their reduced
587 concentrations during the night in EXP1 and EXP2, compared to CTL1 and CTL2 (Fig. 5).
588 The results for the other three cities (Nanjing, Hangzhou, Shanghai) are similar to that of
589 Hefei and are shown in the supporting material (Figure S14a-c).
590 The change of PBL mixing and diurnal variation of primary $PM_{2.5}$ near the surface turn
591 out different DI. Figure 10 shows the diurnal variation of DI of surface $PM_{2.5}$ averaged over
592 the YRD region of East China for January, April, July, and October of 2018 from the
593 observations and the experiments CTL1, CTL2, EXP1, and EXP2. In general, the simulated
594 DI are reduced significantly during the night in EXP1 and EXP2 much more consistent with
595 the observations compared to the ones in CTL1 and CTL2. In spring, the EXP1 and EXP2
596 slightly underestimate DI during night. Figure 11 shows the diurnal variation of DI averaged
597 over the four cities for January, April, July, October of 2018 from the observations and the
598 experiments CTL1, CTL2, EXP1, and EXP2. As discussed above the diurnal variation of DI
599 is much stronger in cities with relatively more emissions. The simulated DI is also more
600 sensitive to the change of PBL mixing coefficient in these four cities compared to that on
601 regional average. The EXP1 and EXP2 produce much more consistent DI with the
602 observations in the four cities than do CTL1 and CTL2 in all seasons. It is also noteworthy
603 that the difference between EXP1 and EXP2 and that between CTL1 and CTL2 is reduced

both on city average and regional average, which indicates that the enhanced PBL exchange coefficient during the night help reduce the modeling sensitivity to the vertical layer configurations. The analysis above suggests that the simulated PBL mixing during the night in the publically-released WRF-Chem may be too weak.

Comparing the simulated surface concentrations of $PM_{2.5}$ components between CTL1 (Fig. 5) and EXP1 (Fig. 9), it can be found that the daily average surface $PM_{2.5}$ mass concentrations should also be reduced when the diurnal variation is reduced due to the reduction of nighttime surface $PM_{2.5}$ concentrations. The model overestimates largely the monthly mean surface $PM_{2.5}$ at the stations of East China in the seasons other than winter from the control experiments. These modeling biases are significantly reduced at most stations of East China (Fig. S15 in the supporting material) in the sensitivity experiments. Figure 12 shows the comparison of monthly mean surface $PM_{2.5}$ concentrations between the observations and the simulations from CTL1 and EXP1 at each observation site over the YRD region of East China for January, April, July, and October of 2018. In all seasons, the CTL1 significantly overestimates the observed surface $PM_{2.5}$ concentrations with the normalized mean biases (NMB) of 22% (winter) - 109% (summer) on regional average. The EXP1 reduces the NMB to 7% (winter) - 38% (summer) on regional average. In CTL1, the NMB of simulation exceeds 50% at 20%, 35%, 65%, and 60% of observational sites over the YRD region of East China in January, April, July, and October, respectively, which reduces to 0%, 10%, 35%, and 20% of all sites in EXP1. In addition, the EXP1 also increases the spatial correlation between observations and simulated results in all seasons (Fig. 12), although with the improvement of modeling diurnal variation the EXP1 still cannot fully capture the observed spatial variability of surface $PM_{2.5}$ concentrations among the observational sites. This may be related to the biases in spatial distributions of emission and model processes contributed to the spatial variability of surface $PM_{2.5}$ concentrations, which deserves further investigation in future.

3.3 Impacts from emission distributions

3.3.1 Impacts from emission diurnal variability

Besides the meteorology such as PBL mixing as discussed above, the diurnal variation of emissions may also play an important role in determining the DI of surface $PM_{2.5}$ concentrations. One sensitivity experiment, EXP1_E1, without diurnal variation of anthropogenic emissions (Fig. 1c) is conducted. Figure 13 shows the spatial distribution of the difference in maximum DI between EXP1 and EXP1_E1 over East China. As removing

diurnal variation of emissions will lead to more emissions during the night and thus increase the DI during the night over polluted area, which generally results in larger maximum DI. Therefore, EXP1 has lower maximum DI than EXP1_E1 over most regions of East China in seasons other than winter. EXP1 could have slightly larger maximum DI in winter when the diurnal variation of DI is relatively small (Fig. 2 and 3) and over the relatively clean region (Fig. 1a) in summer. Figure 14 shows the diurnal index of surface $PM_{2.5}$ concentrations within 24-hour averaged over the four cities for January, April, July, and October of 2018 from observations and the EXP1 and EXP1_E1 experiments. In general, EXP1 shows lower DI than EXP1_E1 during the night, and therefore has smaller diurnal variation of DI in four cities. The largest difference between EXP1 and EXP1_E1 in four cities exists in summer and the smallest is in winter. Comparing to the impacts from PBL mixing as shown in Fig. 11, the reduction of diurnal variation of DI by adding diurnal variation of anthropogenic emissions is much smaller.

Fig. 13 shows that EXP1 with diurnal variation of emissions could simulate slightly larger diurnal variation of DI over the relatively clean region than EXP1_E1 in winter and summer. The higher DI in EXP1 than EXP1_E1 is primarily in the afternoon and evening (Fig. S16 in the supporting material). One grid over south Anhui is selected for analysis of contributions from different processes in the model to the diurnal variation of surface $PM_{2.5}$ concentrations from the experiments EXP1 and EXP1_E1 (Fig. 15). Different from the process contributions over the relatively polluted region (Fig. 8), the contribution from direct local emission to the surface $PM_{2.5}$ concentrations is relatively small over the clean region. Instead, the contributions from chemistry, dry deposition, PBL mixing, and transport dominate the diurnal variation of surface $PM_{2.5}$ concentrations. The PBL mixing could increase the surface $PM_{2.5}$ concentrations during the daytime because of mixing down the pollutants transported from polluted regions above the surface. The diurnal change of surface $PM_{2.5}$ concentrations between EXP1 and EXP1_E1 is very similar with slightly difference that results in their slight difference in DI in the afternoon and night.

3.3.2 Impacts from emission injection height

Previous studies suggested that the injection height of emissions from power plants may also affect the diurnal cycle of surface pollutant concentrations, particularly for SO_2 (e.g., Wang et al.,2010; Lin et al.,2012; Qi et al.,2012; Xu et al.,2014). Therefore, one sensitivity experiment, EXP1_E2, is conducted with setting the anthropogenic emissions placed only in the first layer of model. Figure 16 shows the spatial distribution of the difference in

maximum DI between EXP1 and EXP1_E2 over East China. Over most areas of East China, EXP1 simulates lower maximum DI than EXP1_E2, and the difference is primarily in spring and summer. The impact of injection height is negligible in winter. The distribution of impacts correlates highly with the distribution of power plant locations. The reduction of DI of surface SO_2 concentrations in EXP1 compared to EXP1_E2 is mainly due to more emissions are placed above the PBL during the night (Fig. S17 in the supporting material). As shown in Table 2, most of power plant emissions are placed below 500 m in EXP1. The larger impact in summer than in winter is mainly due to the higher PBL heights during the night in winter (Fig. 7). Therefore, emissions are still placed within the PBL even with the injection height, which results in the small difference of DI of surface SO_2 concentrations between EXP1 and EXP1_E2. For surface $PM_{2.5}$ concentrations, the impact of emission injection height is even smaller and only distinguishable in summer (Fig. S18 in the supporting material). Overall, impact from the injection height of emission on the diurnal variation of surface $PM_{2.5}$ concentrations is much smaller than that from PBL mixing.

4. Summary

In this study, the observed characteristics of diurnal variation of surface $PM_{2.5}$ concentrations over the YRD region of East China in four seasons of 2018 is examined based on the hourly surface observations at 190 stations of the region. On regional average, the observed diurnal variation is the weakest in winter and the strongest in autumn. In spring and autumn, the observed patterns of diurnal variation are similar, showing the minimum surface $PM_{2.5}$ concentration in the afternoon, consistent with previous studies (e.g., Zhang and Cao et al.,2015; Liu et al.,2016; Guo et al.,2017). In summer, different from other seasons, the observed diurnal variation shows the maximum surface $PM_{2.5}$ concentration near the noon time.

The WRF-Chem experiments generally capture the observed seasonality of diurnal variation of surface $PM_{2.5}$ concentrations, except that in summer the model significantly overestimates the diurnal peak during the night and produces opposite diurnal pattern with the minimum concentration near the noon time. The model can generally reproduce the patterns with the minimum noontime concentration in spring and autumn, but overestimates the observed nighttime peaks, particularly in autumn. Emission and PBL mixing are found to be the two dominant processes controlling the diurnal variation of surface $PM_{2.5}$ concentrations over the polluted areas, and the PBL mixing leads to the simulated diurnal

pattern of surface $PM_{2.5}$ concentrations. More specifically, the simulations suggest that the PBL mixing of the primary $PM_{2.5}$ determines the modelled diurnal variation of surface $PM_{2.5}$ concentrations. Although the observation of $PM_{2.5}$ components is not available to evaluate the diurnal variation of primary $PM_{2.5}$, the simulated diurnal variation of surface mixing ratio of CO that is normally used to represent the primary pollutant is compared with the observations (Fig. S19 in the supporting material). The results from experiments with enhanced nighttime PBL mixing are more consistent with the observations compared to the control experiments, which supports the findings about $PM_{2.5}$.

The modeling results are found sensitive to the PBL schemes and the vertical configuration (i.e., the number of model layers within PBL) of simulations. However, none of the PBL schemes in WRF-Chem can reduce the modeling biases in diurnal variation of surface $PM_{2.5}$ concentrations. Contrary to the intuition, more model layers within PBL worsen the model performance, which is mainly due to that more layers within PBL makes the first model layer thinner and enlarges the contribution from emission if PBL mixing is not efficient. The analysis indicates that although PBL height is an important factor to reflect the PBL mixing strength, the PBL mixing process is more explicitly controlled by the PBL mixing coefficient instead of the height in WRF-Chem, particularly during the night. Increasing the lower limit of PBL mixing coefficient within the PBL can significantly reduce the modeling biases in diurnal variation of surface $PM_{2.5}$ concentrations, primarily during the night. In addition, it can also reduce the modeling sensitivity to the model vertical configuration. The model performance of daily mean surface $PM_{2.5}$ concentrations is also largely improved when the biases of diurnal variation are reduced. The diurnal variation of anthropogenic emissions and injection height of power plant emissions can affect the diurnal cycle of surface $PM_{2.5}$ concentrations to some extent, but the impact is much smaller than that of PBL mixing.

5. Discussion

This study highlights the importance of modeling PBL mixing coefficient within PBL in models like WRF-Chem that simulates the PBL mixing process based on the mixing coefficient instead of PBL height. Some studies found that other models also overestimated the diurnal variation of observed surface $PM_{2.5}$ concentrations over East China (e.g., Cai et al.,2011; Liu M et al.,2018). Our finding suggests that those models may also have the problems in modeling PBL mixing during the night. Many of previous

modeling and observation studies focus on investigating the variation of PBL height and its interaction with aerosol concentration (e.g., Sawyer et al., 2015; Ding et al, 2013; Li Z et al, 2017; Song et al.,2018; Su et al., 2018). However, this study reveals that the PBL mixing flux is also critical in addition to the PBL height in terms of understanding the mixing of pollutants within PBL, particularly during the night, which can significantly affect not only the diurnal variation but also the daily mean of surface pollutant concentrations. The increase of PBL mixing during the night reduces the modeling biases, which may suggest that the simulated PBL mixing during the night in WRF-Chem is too weak. One possible reason may be due to urban heat island effect that is not accounted in this study, because the observation sites are mostly at urban or sub-urban areas. The test simulations with the current version of WRF-Chem using Noah land surface model with urban effect can increase the nighttime PBL mixing coefficient from 0.1 m^2/s to 1-10 m^2/s during some cases at urban areas, but the results are sensitive to the urban schemes (not shown), which deserves investigation in future. The model horizontal resolution may also affect the modeling results of PBL mixing and urbanization. However, one sensitivity experiment at 4 km horizontal resolution shows that the PBL mixing at the stations does not change significantly (not shown). The modeling at higher resolution particularly down to large-eddy scale deserves further investigation. Another suggestion is that the PBL mixing of pollutants may not be able to follow directly the mixing coefficient diagnosed by PBL parameterization for meteorology, which deserves further investigation. The improvement of modeling PBL heights is not enough for understanding the PBL mixing of pollutants. In order to better understand PBL structure and detailed mixing process, besides the observation or retrieval of PBL height, observations of PBL characteristics are needed.

Although the sensitivity adjustment of PBL mixing coefficient during the night can largely reduce the modeling biases in diurnal variation of surface $PM_{2.5}$ concentrations, one evident deficiency is that the model produces opposite diurnal pattern compared with observations in summer. It needs to be noted that the WRF-Chem simulations conducted in this study do not consider the SOA production that still has large uncertainties in mechanisms. One sensitivity experiment with the SOA production shows that the model can better represent the observed diurnal pattern of surface $PM_{2.5}$ concentrations in summer showing the maximum concentration in the daytime (Fig. S20 in the supporting material). This indicates that the SOA production may be important for modeling the diurnal variation of surface $PM_{2.5}$ concentrations in summer over East China, which suggests more detailed analysis of impact of SOA production on diurnal cycle of surface $PM_{2.5}$

concentrations is needed with observations. It is also noteworthy that the impact of SOA production on diurnal variation of surface $PM_{2.5}$ concentrations is only significant in summer, likely due to the strong photochemistry activity in summer. Another uncertainty of the results in this study may be related to emissions. Although the diurnal variation and injection height of emission do not contribute significantly to the night time positive biases of surface $PM_{2.5}$ concentrations, the emission uncertainties of primary PM may influence the diurnal cycle of surface $PM_{2.5}$. For example, overestimation of primary PM emission can increase the diurnal variation. Therefore, this study suggests that the long-term measurements of $PM_{2.5}$ components at more stations and the in-situ measurements of vertical profiles of $PM_{2.5}$ concentrations within PBL during the night are needed to further investigate the characteristics of diurnal variation of $PM_{2.5}$, which can improve our understanding of the impacts of multiple processes, such as chemical production, emissions, and meteorology, on the formation and evolution of air pollution.

Data availability

The release version of WRF-Chem can be download from http://www2.mmm.ucar.edu/wrf/users/download/get_source.html. The updated USTC version of WRF-Chem can be downloaded from http://aemol.ustc.edu.cn/product/list/ or contact chunzhao@ustc.edu.cn. Also, the code modifications will be incorporated the release version of WRF-Chem in future.

Author contributions

Qiuyan Du and Chun Zhao designed the experiments, conducted and analyzed the simulations. All authors contributed to the discussion and final version of the paper.

Acknowledgements

This research was supported by the Fundamental Research Funds for the Central Universities, and the National Natural Science Foundation of China (grant 41775146). The study used the computing resources from the High-Performance Computing Center of University of Science and Technology of China (USTC). Part of the observation data is from the Qingyue Open Environmental Data Center (https://data.epmap.org).

804

805 # Reference

806 Ackerman, T. P.: A Model of the Effect of Aerosols on Urban Climates with Particular
807 Applications to the Los Angeles Basin, J. Atmos. Sci., 34, 531–547,
808 doi:10.1175/1520-0469(1977)034<0531:AMOTEO>2.0.CO;2, 1977.
809 Arola, A., Eck, T. F., Huttunen, J., Lehtinen, K. E. J., Lindfors, A. V., Myhre, G., Smirnov,
810 A., Tripathi, S. N., and Yu, H.: Influence of observed diurnal cycles of aerosol optical
811 depth on aerosol direct radiative effect, Atmos. Chem. Phys., 13, 7895-7901, 2013.
812 Bacmeister, J. T., Wehner, M. F., Neale, R. B., Gettelman, A., Hannay, C., Lauritzen, P. H.,
813 Caron, J. M., and Truesdale, J. E.: Exploratory High-Resolution Climate Simulations
814 using the Community Atmosphere Model (CAM), J. Climate, 27, 3073–3099,
815 doi:10.1175/JCLI-D-13-00387.1, 2014.
816 Barnard, J. C., Fast, J. D., Paredes-Miranda, G., Arnott, W. P., and Laskin, A.: Technical
817 Note: Evaluation of the WRF-Chem "Aerosol Chemical to Aerosol Optical
818 Properties" Module using data from the MILAGRO campaign, Atmos. Chem. Phys.,
819 10, 7325–7340, doi:10.5194/acp-10-7325-2010, 2010.
820 Bei, N., Li, G., Huang, R., Cao, J., Meng, N., Feng, T., Liu, S., Zhang, T., Zhang, Q., and
821 Molina, L. T.: Typical synoptic situations and their impacts on the wintertime air
822 pollution in the Guanzhong basin, China, Atmos. Chem. Phys., 16, e7387, 2016.
823 Binkowski, F. S. and Shankar, U.: The Regional Particulate Matter Model: 1. Model
824 Description and Preliminary Results, J. Geophys. Res., 100, 26191–26209, 1995.
825 Cai, H. and Xie, S.: Traffic-related air pollution modeling during the 2008 Beijing
826 Olympic Games: the effects of an odd-even day traffic restriction scheme, The
827 Science of the total environment, 409, 1935–1948,
828 doi:10.1016/j.scitotenv.2011.01.025, 2011.
829 Chapman, E. G., Gustafson, W. I., Easter, R. C., Barnard, J. C., Ghan, S. J., Pekour, M. S.,
830 and Fast, J. D.: Coupling aerosol-cloud-radiative processes in the WRF-Chem model:
831 investigating the radiative impact of elevated point sources, Atmos. Chem. Phys., 9,
832 945-964, 2008.
833 Chen, D., Cui, H., Zhao, Y., Yin, L., Lu, Y., and Wang, Q.: A two-year study of
834 carbonaceous aerosols in ambient $PM_{2.5}$ at a regional background site for western
835 Yangtze River Delta, China, Atmospheric Research, 183, 351–361,
836 doi:10.1016/j.atmosres.2016.09.004, 2017.

837 Chen, S., Zhao, C., Qian, Y., Leung, L. R., Huang, J., Huang, Z., Bi, J., Zhang, W., Shi, J.,
838 Yang, L., Li, D., and Li, J.: Regional modeling of dust mass balance and radiative
839 forcing over East Asia using WRF-Chem, Aeolian Research, 15, 15–30,
840 doi:10.1016/j.aeolia.2014.02.001, 2014.
841 Chen, T., He, J., Lu, X., She, J., and Guan, Z.: Spatial and Temporal Variations of $PM_{2.5}$
842 and Its Relation to Meteorological Factors in the Urban Area of Nanjing, China,
843 International journal of environmental research and public health, 13,
844 doi:10.3390/ijerph13090921, 2016.
845 Chen, W., Tang, H., and Zhao, H.: Diurnal, weekly and monthly spatial variations of air
846 pollutants and air quality of Beijing, Atmospheric Environment, 119, 21–34,
847 doi:10.1016/j.atmosenv.2015.08.040, 2015.
848 Cheng, Y., Zheng, G., Wei, C., Mu, Q., Zheng, B., Wang, Z., Gao, M., Zhang, Q., He, K.,
849 Carmichael, G., Pöschl, U., and Su, H.: Reactive nitrogen chemistry in aerosol water
850 as a source of sulfate during haze events in China, Science advances, 2, e1601530,
851 doi:10.1126/sciadv.1601530, 2016.
852 Davidson C I, Phalen R F, Solomon P A.: Airborne particulate matter and human health: A
853 review, 39(8), 737–749, 2005.
854 Dentener, F., Kinne, S., Bond, T., Boucher, O., Cofala, J., Generoso, S., Ginoux, P., Gong,
855 S., Hoelzemann, J. J., Ito, A., Marelli, L., Penner, J. E., Putaud, J.-P., Textor, C.,
856 Schulz, M., van der Werf, G. R., and Wilson, J.: Emissions of primary aerosol and
857 precursor gases in the years 2000 and 1750, prescribed data-sets for AeroCom, Atmos.
858 Chem. Phys., 6, 4321-4344, 2006.
859 Dickerson, R. R., Kondragunta, S., Stenchikov, G., Civerolo, K. L., Doddridge, B. G., and
860 Holben, B. N.: The impact of aerosols on solar ultraviolet radiation and
861 photochemical smog, Science (New York, N.Y.), 278, 827–830,
862 doi:10.1126/science.278.5339.827, 1997.
863 Ding, A. J., Fu, C. B., Yang, X. Q., Sun, J. N., Petäjä, T., Kerminen, V. M., Wang, T., Xie,
864 Y., Herrmann, E., Zheng, L. F., Nie, W., Liu, Q., Wei, X. L., Kulmala, M.: Intense
865 atmospheric pollution modifies weather: a case of mixed biomass burning with fossil
866 fuel combustion pollution in eastern China, Atmospheric Chemistry and Physics, 13,
867 10545–10554, 2013.
868 Du, Q., Faber, V., & Gunzburger, M.: Centroidal Voronoi tessellations: Applications and
869 algorithms, SIAM review, 41, 637–676, 1999.

Easter, R. C., Ghan, S. J., Zhang, Y., Saylor, R. D., Chapman, E. G., Laulainen, N. S., Abdul-Razzak, H., Leung, L. R., Bian, X., and Zaveri, R. A.: MIRAGE: Model Description and Evaluation of Aerosols and Trace Gases, J. Geophys. Res., 109, D20210, doi:10.1029/2004JD004571, 2004.

Fast, J. D, Gustafson Jr., W. I., Easter, R. C., Zaveri, R. A., Barnard, J. C., Chapman, E. G., and Grell, G. A.: Evolution of ozone, particulates, and aerosol direct forcing in an urban area using a new fully-coupled meteorology, chemistry, and aerosol model, J. Geophys. Res., 111, D21305, doi:10.1029/2005JD006721, 2006.

Feng, J., Zhong, M., Xu, B., Du, Y., Wu, M., Wang, H., and Chen, C.: Concentrations, seasonal and diurnal variations of black carbon in $PM_{2.5}$ in Shanghai, China, Atmospheric Research, 147-148, 1–9, doi:10.1016/j.atmosres.2014.04.018, 2014.

Fu, Q., Zhuang, G., Wang, J., Xu, C., Huang, K., Li, J., Hou, B., Lu, T., and Streets, D. G.: Mechanism of formation of the heaviest pollution episode ever recorded in the Yangtze River Delta, China, Atmospheric Environment, 42, 2023–2036, doi:10.1016/j.atmosenv.2007.12.002, 2008.

Gakidou, E., Afshin, A., Abajobir, A. A., Abate, K. H., Abbafati, C., Abbas, K. M., ... & Abu-Raddad, L.: Global, regional, and national comparative risk assessment of 84 behavioural, environmental and occupational, and metabolic risks or clusters of risks, 1990–2016: a systematic analysis for the Global Burden of Disease Study 2016, The Lancet, 390, 1345-1422, 2017.

Gao, Y., Liu, X., Zhao, C., and Zhang, M.: Emission controls versus meteorological conditions in determining aerosol concentrations in Beijing during the 2008 Olympic Games, Atmos. Chem. Phys., 11, 12437–12451, doi:10.5194/acp-11-12437-2011, 2011.

Gao, Y., Zhao, C., Liu, X., Zhang, M., and Leung, L. R.: WRF-Chem simulations of aerosols and anthropogenic aerosol radiative forcing in East Asia, Atmospheric Environment, 92, 250–266, doi:10.1016/j.atmosenv.2014.04.038, 2014.

Geng, G., Zhang, Q., Martin, R. V., van Donkelaar, A., Huo, H., Che, H., Lin, J., and He, K.: Estimating long-term $PM_{2.5}$ concentrations in China using satellite-based aerosol optical depth and a chemical transport model, Remote Sensing of Environment, 166, 262–270, doi:10.1016/j.rse.2015.05.016, 2015.

Ginoux, P., Chin, M., Tegen, I., Prospero, J. M., Holben, B., Dubovik, O., and Lin, S.: Sources and distributions of dust aerosols simulated with the GOCART model, J. Geophys. Res., 106, 20225–20273, 2001.

Gong, D.Y., Ho, C.-H., Chen, D., Qian, Y., Choi, Y.-S., and Kim, J.: Weekly cycle of aerosol-meteorology interaction over China, J. Geophys. Res., 112, L03819, doi:10.1029/2007JD008888, 2007.

Gong, S. L.: A parameterization of sea-salt aerosol source function for sub- and super-micron particles, Global Biogeochem. Cycles, 17, n/a-n/a, doi:10.1029/2003GB002079, 2003.

Grell, G. A., Peckham, S. E., Schmitz, R., and McKeen, S. A., Frost, G., Skamarock, W. C., and Eder, B.: Fully coupled "online" chemistry within the WRF model, Atmos. Environ., 39, 6957–6976, 2005.

Gu, Z., Feng, J., Han, W., Li, L., Wu, M., Fu, J., and Sheng, G.: Diurnal variations of polycyclic aromatic hydrocarbons associated with $PM_{2.5}$ in Shanghai, China, Journal of environmental sciences (China), 22, 389–396, 2010.

Guo J, Miao Y, Zhang Y, et al.: The climatology of planetary boundary layer height in China derived from radiosonde and reanalysis data, Atmospheric Chemistry and Physics, 16(20): 13309, 2016.

Guo, H., Cheng, T., Gu, X., Wang, Y., Chen, H., Bao, F., Shi, S., Xu, B., Wang, W., Zuo, X., Zhang, X., and Meng, C.: Assessment of $PM_{2.5}$ concentrations and exposure throughout China using ground observations, The Science of the total environment, 601-602, 1024–1030, doi:10.1016/j.scitotenv.2017.05.263, 2017.

Guo, J., Xia, F., Zhang, Y., Liu, H., Li, J., Lou, M., He, J., Yan, Y., Wang, F., Min, M., and Zhai, P.: Impact of diurnal variability and meteorological factors on the $PM_{2.5}$ - AOD relationship: Implications for $PM_{2.5}$ remote sensing, Environmental pollution (Barking, Essex 1987), 221, 94–104, doi:10.1016/j.envpol.2016.11.043, 2017.

Gustafson, W. I., Chapman, E. G., Ghan, S. J., Easter, R. C., and Fast, J. D.: Impact on modeled cloud characteristics due to simplified treatment of uniform cloud condensation nuclei during NEAQS 2004, Geophys. Res. Lett., 34, L19809, doi:10.1029/2007GL030021, 2007.

Ho, H. C., Wong, M. S., Yang, L., Shi, W., Yang, J., Bilal, M., and Chan, T.-C.: Spatiotemporal influence of temperature, air quality, and urban environment on cause-specific mortality during hazy days, Environment international, 112, 10–22, doi:10.1016/j.envint.2017.12.001, 2018.

Hong, S.-Y., Noh, Y., and Dudhia, J.: A New Vertical Diffusion Package with an Explicit Treatment of Entrainment Processes, Mon. Wea. Rev., 134, 2318–2341, doi:10.1175/MWR3199.1, 2006.

938 Hu, J., Chen, J., Ying, Q., and Zhang, H.: One-Year Simulation of Ozone and Particulate
939 Matter in China Using WRF/CMAQ Modeling System, Atmos. Chem. Phys., 16,
940 10333, 2016.
941 Hu, J., Wang, Y., Ying, Q., and Zhang, H.: Spatial and temporal variability of $PM_{2.5}$ and
942 PM_{10} over the North China Plain and the Yangtze River Delta, China, Atmospheric
943 Environment, 95, 598–609, doi:10.1016/j.atmosenv.2014.07.019, 2014.
944 Hu, Z., Huang, J., Zhao, C., Bi, J., Jin, Q., Qian, Y., Leung, L. R., Feng, T., Chen, S., and
945 Ma, J.: Modeling the contributions of Northern Hemisphere dust sources to dust
946 outflow from East Asia, Atmospheric Environment, 202, 234–243,
947 doi:10.1016/j.atmosenv.2019.01.022, 2019.
948 Hu, Z., Zhao, C., Huang, J., Leung, L. R., Qian, Y., Yu, H., Huang, L., and Kalashnikova,
949 O. V.: Trans-pacific transport and evolution of aerosols: Evaluation of quasi global
950 WRF-Chem simulation with multiple observations, Geosci. Model Dev. Discuss.,
951 1–65, doi:10.5194/gmd-2015-248, 2016.
952 Huang, G., Cheng, T., Zhang, R., Tao, J., Leng, C., Zhang, Y., Zha, S., Zhang, D., Li, X.,
953 and Xu, C.: Optical properties and chemical composition of $PM_{2.5}$ in Shanghai in the
954 spring of 2012, Particuology, 13, 52–59, doi:10.1016/j.partic.2013.10.005, 2014.
955 Huang, X., Ding, A., Liu, L., Liu, Q., Ding, K., Nie, W., Xu, Z., Chi, X., Wang, M., Sun, J.,
956 Guo, W., and Fu, C.: Effects of aerosol-radiation interaction on precipitation during
957 biomass-burning season in East China, Atmos. Chem. Phys., 16, 2016.
958 Huang, X.F., He, L.Y., Hu, M., Canagaratna, M. R., Sun, Y., Zhang, Q., Zhu, T., Xue, L.,
959 Zeng, L.-W., Liu, X.-G., Zhang, Y.-H., Jayne, J. T., Ng, N. L., and Worsnop, D. R.:
960 Highly time-resolved chemical characterization of atmospheric submicron particles
961 during 2008 Beijing Olympic Games using an Aerodyne High-Resolution Aerosol
962 Mass Spectrometer, Atmos. Chem. Phys., 10, 8933-8945, 2010.
963 Iacono, M. J., Mlawer, E. J., Clough, S. A., & Morcrette, J. J.: Impact of an improved
964 longwave radiation model, RRTM, on the energy budget and thermodynamic
965 properties of the NCAR community climate model, CCM3, Journal of Geophysical
966 Research: Atmospheres, 105, 14873-14890, 2000.
967 Jacobson, M. Z.: Studying the effects of aerosols on vertical photolysis rate coefficient and
968 temperature profiles over an urban airshed, J. Geophys. Res., 103, 10593–10604,
969 doi:10.1029/98JD00287, 1998.

970 Jaeglé, L., Quinn, P. K., Bates, T. S., Alexander, B., & Lin, J. T.: Global distribution of sea
971 salt aerosols: new constraints from in situ and remote sensing observations,
972 Atmospheric Chemistry and Physics, 11, 3137-3157, 2011.
973 Janssens-Maenhout, G., Crippa, M., Guizzardi, D., Dentener, F., Muntean, M., Pouliot, G.,
974 Keating, T., Zhang, Q., Kurokawa, J., Wankmüller, R., van der Denier Gon, H.,
975 Klimont, Z., Frost, G., Darras, S., and Koffi, B.: HTAP_v2: a mosaic of regional and
976 global emission gridmaps for 2008 and 2010 to study hemispheric transport of air
977 pollution, Atmos. Chem. Phys. Discuss., 15, 12867–12909,
978 doi:10.5194/acpd-15-12867-2015, 2015.
979 Jia, M., Zhao, T., Cheng, X., Gong, S., Zhang, X., Tang, L., Liu, D., Wu, X., Wang, L.,
980 and Chen, Y.: Inverse Relations of $PM_{2.5}$ and O_3 in Air Compound Pollution between
981 Cold and Hot Seasons over an Urban Area of East China, Atmosphere, 8, 59,
982 doi:10.3390/atmos8030059, 2017.
983 Jiang, F., Liu, Q., Huang, X., Wang, T., Zhuang, B., and Xie, M.: Regional modeling of
984 secondary organic aerosol over China using WRF/Chem, Journal of Aerosol Science,
985 43, 57–73, doi:10.1016/j.jaerosci.2011.09.003, 2012.
986 Kain, J. S.: The Kain–Fritsch convective parameterization: An update, J. Appl. Meteorol.,
987 43, 170–181, 2004.
988 Kassianov, E., Barnard, J., Pekour, M., Berg, L. K., Michalsky, J., Lantz, K., and Hodges,
989 G.: Do diurnal aerosol changes affect daily average radiative forcing?, Geophys. Res.
990 Lett., 40, 3265–3269, doi:10.1002/grl.50567, 2013.
991 Kok, J. F.: A scaling theory for the size distribution of emitted dust aerosols suggests
992 climate models underestimate the size of the global dust cycle, Proceedings of the
993 National Academy of Sciences of the United States of America, 108, 1016–1021,
994 doi:10.1073/pnas.1014798108, 2011.
995 Kuang, Y., Zhao, C. S., Tao, J. C., and Ma, N.: Diurnal variations of aerosol optical
996 properties in the North China Plain and their influences on the estimates of direct
997 aerosol radiative effect, Atmos. Chem. Phys., 15, 5761–5772,
998 doi:10.5194/acp-15-5761-2015, 2015.
999 Li, G., Wang, Y., Lee, K. H., Diao, Y., & Zhang, R.: Impacts of aerosols on the
1000 development and precipitation of a mesoscale squall line, Journal of Geophysical
1001 Research: Atmospheres, 114, 2009.
1002 Li, J., Wang, G., Aggarwal, S. G., Huang, Y., Ren, Y., Zhou, B., Singh, K., Gupta, P. K.,
1003 Cao, J., and Zhang, R.: Comparison of abundances, compositions and sources of

elements, inorganic ions and organic compounds in atmospheric aerosols from Xi'an and New Delhi, two megacities in China and India, The Science of the total environment, 476-477, 485–495, doi:10.1016/j.scitotenv.2014.01.011, 2014.

Li, J., Yang, W., Wang, Z., Chen, H., Hu, B., Li, J., Sun, Y., Fu, P., and Zhang, Y.: Modeling study of surface ozone source-receptor relationships in East Asia, Atmospheric Research, 167, 77–88, doi:10.1016/j.atmosres.2015.07.010, 2016.

Li, M., Liu, H., Geng, G., Hong, C., Liu, F., Song, Y., ... & Zhang, Q.: Anthropogenic emission inventories in China: a review, National Science Review, 4, 834-866, 2017a.

Li, M., Zhang, Q., Kurokawa, J.-i., Woo, J.-H., He, K., Lu, Z., Ohara, T., Song, Y., Streets, D. G., Carmichael, G. R., Cheng, Y., Hong, C., Huo, H., Jiang, X., Kang, S., Liu, F., Su, H., and Zheng, B.: MIX: a mosaic Asian anthropogenic emission inventory under the international collaboration framework of the MICS-Asia and HTAP, Atmos. Chem. Phys., 17, 935–963, doi:10.5194/acp-17-935-2017, 2017b.

Li, P., Wang, L., Guo, P., Yu, S., Mehmood, K., Wang, S., Liu, W., Seinfeld, J. H., Zhang, Y., Wong, D. C., Alapaty, K., Pleim, J., and Mathur, R.: High reduction of ozone and particulate matter during the 2016 G-20 summit in Hangzhou by forced emission controls of industry and traffic, Environ Chem Lett, 15, 709–715, doi:10.1007/s10311-017-0642-2, 2017.

Li, R., Li, Z., Gao, W., Ding, W., Xu, Q., & Song, X.: Diurnal, seasonal, and spatial variation of $PM_{2.5}$ in Beijing, Science Bulletin, 60, 387-395, 2015.

Li, T., Horton, R. M., Bader, D. A., Liu, F., Sun, Q., and Kinney, P. L.: Long-term projections of temperature-related mortality risks for ischemic stroke, hemorrhagic stroke, and acute ischemic heart disease under changing climate in Beijing, China, Environment international, 112, 1–9, doi:10.1016/j.envint.2017.12.006, 2018.

Li, X., Zhang, Q., Zhang, Y., Zheng, B., Wang, K., Chen, Y., Wallington, T. J., Han, W., Shen, W., Zhang, X., and He, K.: Source contributions of urban $PM_{2.5}$ in the Beijing–Tianjin–Hebei region: Changes between 2006 and 2013 and relative impacts of emissions and meteorology, Atmospheric Environment, 123, 229–239, doi:10.1016/j.atmosenv.2015.10.048, 2015.

Li, Z., Guo, J., Ding, A., Liao, H., Liu, J., Sun, Y., ... & Zhu, B.: Aerosol and boundary-layer interactions and impact on air quality, National Science Review, 4, 810-833, 2017.

Liao, J., Wang, T., Wang, X., Xie, M., Jiang, Z., Huang, X., and Zhu, J.: Impacts of different urban canopy schemes in WRF/Chem on regional climate and air quality in

1038 Yangtze River Delta, China, Atmospheric Research, 145-146, 226–243,
1039 doi:10.1016/j.atmosres.2014.04.005, 2014.
1040 Lin, M., Tao, J., Chan, C.-Y., Cao, J.-J., Zhang, Z.-S., Zhu, L.-H., and Zhang, R.-J.:
1041 Regression Analyses between Recent Air Quality and Visibility Changes in
1042 Megacities at Four Haze Regions in China, Aerosol Air Qual. Res., 12, 1049–1061,
1043 doi:10.4209/aaqr.2011.11.0220, 2012.
1044 Lin, W., Xu, X., Ma, Z., Zhao, H., Liu, X., and Wang, Y.: Characteristics and recent trends
1045 of sulfur dioxide at urban, rural, and background sites in north China: effectiveness of
1046 control measures, Journal of environmental sciences (China), 24, 34–49, 2012.
1047 Liu, J., Li, J., and Li, W.: Temporal Patterns in Fine Particulate Matter Time Series in
1048 Beijing: A Calendar View, Scientific reports, 6, 32221, doi:10.1038/srep32221, 2016.
1049 Liu, M., Lin, J., Wang, Y., Sun, Y., Zheng, B., Shao, J., ... & Yan, Y.: Spatiotemporal
1050 variability of NO_2 and $PM_{2.5}$ over Eastern China: observational and model analyses
1051 with a novel statistical method, Atmospheric Chemistry and Physics, 18,
1052 12933-12952, 2018.
1053 Liu, S., Hua, S., Wang, K., Qiu, P., Liu, H., Wu, B., Shao, P., Liu, X., Wu, Y., Xue, Y.,
1054 Hao, Y., and Tian, H.: Spatial-temporal variation characteristics of air pollution in
1055 Henan of China: Localized emission inventory, WRF/Chem simulations and potential
1056 source contribution analysis, The Science of the total environment, 624, 396–406,
1057 doi:10.1016/j.scitotenv.2017.12.102, 2018.
1058 Liu, T., Cai, Y., Feng, B., Cao, G., Lin, H., Xiao, J., Li, X., Liu, S., Pei, L., Fu, L., Yang,
1059 X., Zhang, B., and Ma, W.: Long-term mortality benefits of air quality improvement
1060 during the twelfth five-year-plan period in 31 provincial capital cities of China,
1061 Atmospheric Environment, 173, 53–61, doi:10.1016/j.atmosenv.2017.10.054, 2018.
1062 Liu, X.-Y., Zhang, Y., Zhang, Q., and He, K.-B.: Application of online-coupled
1063 WRF/Chem-MADRID in East Asia: Model evaluation and climatic effects of
1064 anthropogenic aerosols, Atmospheric Environment, 124, 321–336,
1065 doi:10.1016/j.atmosenv.2015.03.052, 2016.
1066 Ma, Q., Wu, Y., Tao, J., Xia, Y., Liu, X., Zhang, D., Han, Z., Zhang, X., and Zhang, R.:
1067 Variations of Chemical Composition and Source Apportionment of $PM_{2.5}$ during
1068 Winter Haze Episodes in Beijing, Aerosol Air Qual. Res., 17, 2791–2803,
1069 doi:10.4209/aaqr.2017.10.0366, 2017.

Ma, Y., Xu, X., Song, W., Geng, F., and Wang, L.: Seasonal and diurnal variations of particulate organosulfates in urban Shanghai, China, Atmospheric Environment, 85, 152–160, doi:10.1016/j.atmosenv.2013.12.017, 2014.

Mellor G L, Yamada T.: Development of a turbulence closure model for geophysical fluid problems, Reviews of Geophysics, 20(4): 851-875, 1982.

Menut, L., Goussebaile, A., Bessagnet, B., Khvorostiyanov, D., and Ung, A.: Impact of realistic hourly emissions profiles on air pollutants concentrations modelled with CHIMERE, Atmospheric Environment, 49, 233–244, doi:10.1016/j.atmosenv.2011.11.057, 2012.

Miao, Y., Guo, J., Liu, S., Zhao, C., Li, X., Zhang, G., Wei, W., and Ma, Y.: Impacts of synoptic condition and planetary boundary layer structure on the trans-boundary aerosol transport from Beijing-Tianjin-Hebei region to northeast China, Atmospheric Environment, 181, 1–11, doi:10.1016/j.atmosenv.2018.03.005, 2018.

Mlawer, E. J., S. J. Taubman, P. D. Brown, M. J. Iacono, and S. A. Clough.: Radiative transfer for inhomogeneous atmosphere: RRTM, a validated correlated-k model for the longwave, J. Geophys. Res., **102**, 16 663–16 682, 1997.

Morrison, H., Thompson, G., and Tatarskii, V.: Impact of Cloud Microphysics on the Development of Trailing Stratiform Precipitation in a Simulated Squall Line: Comparison of One- and TwoMoment Schemes, Mon. Weather Rev., 137, 991–1007, 2009.

Nakanishi, M. and Niino, H.: An Improved Mellor–Yamada Level-3 Model: Its Numerical Stability and Application to a Regional Prediction of Advection Fog, Boundary-Layer Meteorol, 119, 397–407, doi:10.1007/s10546-005-9030-8, 2006.

Ni, Z.-Z., Luo, K., Zhang, J.-X., Feng, R., Zheng, H.-X., Zhu, H.-R., Wang, J.-F., Fan, J.-R., Gao, X., and Cen, K.-F.: Assessment of winter air pollution episodes using long-range transport modeling in Hangzhou, China, during World Internet Conference, 2015, Environmental pollution (Barking, Essex 1987), 236, 550–561, doi:10.1016/j.envpol.2018.01.069, 2018.

Noh, Y., W.-G. Cheon, S.-Y. Hong, and S. Raasch.: Improvement of the K-profile model for the planetary boundary layer based on large eddy simulation data, Bound.-Layer Meteor., 107, 401–427, doi:10.1023/A:1022146015946, 2003.

Olivier, J., Peters, J., Granier, C., Petron, G., Muller, J. F., and Wallens, S.: Present and Future surface emissions of anthropogenic compounds, POET report #2, EU project EVK2-1999-00011, 2003.

Pal, S., Lee, T. R., Phelps, S., and Wekker, S. F. J. de: Impact of atmospheric boundary layer depth variability and wind reversal on the diurnal variability of aerosol concentration at a valley site, The Science of the total environment, 496, 424–434, doi:10.1016/j.scitotenv.2014.07.067, 2014.

Pathak, R. K., Wang, T., and Wu, W. S.: Nighttime enhancement of $PM_{2.5}$ nitrate in ammonia-poor atmospheric conditions in Beijing and Shanghai: Plausible contributions of heterogeneous hydrolysis of N_2O_5 and HNO_3 partitioning, Atmospheric Environment, 45, 1183–1191, doi:10.1016/j.atmosenv.2010.09.003, 2011.

Petäjä, T., Järvi, L., Kerminen, V.-M., Ding, A. J., Sun, J. N., Nie, W., Kujansuu, J., Virkkula, A., Yang, X.-Q., Fu, C. B., Zilitinkevich, S., and Kulmala, M.: Enhanced air pollution via aerosol-boundary layer feedback in China, Scientific reports, 6, 18998, doi:10.1038/srep18998, 2016.

Pope III C A, Dockery D W.: Health effects of fine particulate air pollution: lines that connect, Journal of the air & waste management association, 56, 709-742, 2006.

Powers, J. G., et al.: THE WEATHER RESEARCH AND FORECASTING MODEL Overview, System Efforts, and Future Directions, Bull. Amer. Meteorol. Soc., 98(8), 1717-1737, doi:10.1175/bams-d-15-00308.1, 2017.

Qi, H., Lin, W., Xu, X., Yu, X., and Ma, Q.: Significant downward trend of SO_2 observed from 2005 to 2010 at a background station in the Yangtze Delta region, China, Sci. China Chem., 55, 1451–1458, doi:10.1007/s11426-012-4524-y, 2012.

Quan, J., Gao, Y., Zhang, Q., Tie, X., Cao, J., Han, S., Meng, J., Chen, P., and Zhao, D.: Evolution of planetary boundary layer under different weather conditions, and its impact on aerosol concentrations, Particuology, 11, 34–40, doi:10.1016/j.partic.2012.04.005, 2013.

Roig Rodelas, R., Perdrix, E., Herbin, B., and Riffault, V.: Characterization and variability of inorganic aerosols and their gaseous precursors at a suburban site in northern France over one year (2015–2016), Atmospheric Environment, 200, 142–157, doi:10.1016/j.atmosenv.2018.11.041, 2019.

Sawyer V R. Interaction between aerosol and the planetary boundary layer depth at sites in the US and China[C]//AGU Fall Meeting Abstracts. 2015.

Seaman, N. L., Stauffer, D. R., and Lario-Gibbs, A. M.: A Multiscale Four-Dimensional Data Assimilation System Applied in the San Joaquin Valley during SARMAP. Part I:

Modeling Design and Basic Performance Characteristics, J. Appl. Meteor., 34, 1739–1761, doi:10.1175/1520-0450(1995)034<1739:AMFDDA>2.0.CO;2, 1995.

Seaton, A., MacNee, W., Donaldson, K., and Godden, D.: Particulate air pollution and acute health effects, Lancet (London, England), 345, 176–178, doi:10.1016/s0140-6736(95)90173-6, 1995.

Shao, J., Chen, Q., Wang, Y., Lu, X., He, P., Sun, Y., Shah, V., Martin, R. V., Philip, S., Song, S., Zhao, Y., Xie, Z., Zhang, L., and Alexander, B.: Heterogeneous sulfate aerosol formation mechanisms during wintertime Chinese haze events: air quality model assessment using observations of sulfate oxygen isotopes in Beijing, Atmos. Chem. Phys., 19, 6107–6123, doi:10.5194/acp-19-6107-2019, 2019.

Skamarock W C, Klemp J B, Dudhia J, et al. A description of the Advanced Research WRF version 3. NCAR Technical note-475+ STR[J]. 2008.

Song, J., Xia, X., Che, H., Wang, J., Zhang, X., and Li, X.: Daytime variation of aerosol optical depth in North China and its impact on aerosol direct radiative effects, Atmospheric Environment, 182, 31–40, doi:10.1016/j.atmosenv.2018.03.024, 2018.

Stauffer, D. R. and Seaman, N. L.: Use of four-dimensional data assimilation in a limited-area mesoscale model, Part I: Experiments with synoptic-scale data, Mon. Weather Rev., 118, 1250–1277, 1990.

Su, T., Li, Z., and Kahn, R.: Relationships between the planetary boundary layer height and surface pollutants derived from lidar observations over China, Atmos. Chem. Phys., 18, 15921-15935, 2018.

Sun, Y. L., Wang, Z. F., Du, W., Zhang, Q., Wang, Q. Q., Fu, P. Q., Pan, X. L., Li, J., Jayne, J., and Worsnop, D. R.: Long-term real-time measurements of aerosol particle composition in Beijing, China: seasonal variations, meteorological effects, and source analysis, Atmos. Chem. Phys., 15, 10149-10165, 2015.

Tao, M., Chen, L., Li, R., Wang, L., Wang, J., Wang, Z., Tang, G., and Tao, J.: Spatial oscillation of the particle pollution in eastern China during winter: Implications for regional air quality and climate, Atmospheric Environment, 144, 100–110, doi:10.1016/j.atmosenv.2016.08.049, 2016.

Tao, W., Liu, J., Ban-Weiss, G. A., Hauglustaine, D. A., Zhang, L., Zhang, Q., Cheng, Y., Yu, Y., and Tao, S.: Effects of urban land expansion on the regional meteorology and air quality of Eastern China, Atmos. Chem. Phys., 15, 8597-8614, 2015.

1169 Tiwari, S., Srivastava, A. K., Bisht, D. S., Parmita, P., Srivastava, M. K., and Attri, S. D.:
1170 Diurnal and seasonal variations of black carbon and $PM_{2.5}$ over New Delhi, India:
1171 Influence of meteorology, Atmospheric Research, 125-126, 50–62,
1172 doi:10.1016/j.atmosres.2013.01.011, 2013.
1173 Verma, V., Ning, Z., Cho, A. K., Schauer, J. J., Shafer, M. M., and Sioutas, C.: Redox
1174 activity of urban quasi-ultrafine particles from primary and secondary sources,
1175 Atmospheric Environment, 43, 6360–6368, doi:10.1016/j.atmosenv.2009.09.019,
1176 2009.
1177 Wang, G., Zhang, R., Gomez, M. E., Yang, L., Levy Zamora, M., Hu, M., Lin, Y., Peng, J.,
1178 Guo, S., Meng, J., Li, J., Cheng, C., Hu, T., Ren, Y., Wang, Y., Gao, J., Cao, J., An,
1179 Z., Zhou, W., Li, G., Wang, J., Tian, P., Marrero-Ortiz, W., Secrest, J., Du, Z., Zheng,
1180 J., Shang, D., Zeng, L., Shao, M., Wang, W., Huang, Y., Wang, Y., Zhu, Y., Li, Y.,
1181 Hu, J., Pan, B., Cai, L., Cheng, Y., Ji, Y., Zhang, F., Rosenfeld, D., Liss, P. S., Duce,
1182 R. A., Kolb, C. E., and Molina, M. J.: Persistent sulfate formation from London Fog
1183 to Chinese haze, Proceedings of the National Academy of Sciences of the United
1184 States of America, 113, 13630–13635, doi:10.1073/pnas.1616540113, 2016.
1185 Wang, J., Christopher, S. A., Nair, U. S., Reid, J. S., Prins, E. M., Szykman, J., & Hand, J.
1186 L.: Mesoscale modeling of Central American smoke transport to the United States:
1187 1."Top-down" assessment of emission strength and diurnal variation impacts, Journal
1188 of Geophysical Research: Atmospheres, 111, 2006.
1189 Wang, T., Jiang, F., Deng, J., Shen, Y., Fu, Q., Wang, Q., Fu, Y., Xu, J., and Zhang, D.:
1190 Urban air quality and regional haze weather forecast for Yangtze River Delta region,
1191 Atmospheric Environment, 58, 70–83, doi:10.1016/j.atmosenv.2012.01.014, 2012.
1192 Wang, X., Liang, X.-Z., Jiang, W., Tao, Z., Wang, J. X.L., Liu, H., Han, Z., Liu, S., Zhang,
1193 Y., and Grell, G. A.: WRF-Chem simulation of East Asian air quality: Sensitivity to
1194 temporal and vertical emissions distributions, Atmospheric Environment, 44, 660–669,
1195 doi:10.1016/j.atmosenv.2009.11.011, 2010.
1196 Wang, X.P., Mauzerall, D. L., Hu, Y., Russell, A. G., Larson, E. D., Woo, J.-H., Streets, D.
1197 G., and Guenther, A.: A high-resolution emission inventory for eastern China in 2000
1198 and three scenarios for 2020, Atmospheric Environment, 39, 5917–5933,
1199 doi:10.1016/j.atmosenv.2005.06.051, 2005.
1200 Wang, Y.G., Ying, Q., Hu, J., and Zhang, H.: Spatial and temporal variations of six criteria
1201 air pollutants in 31 provincial capital cities in China during 2013–2014, Environment
1202 international, 73, 413–422, doi:10.1016/j.envint.2014.08.016, 2014.

Wang, Y.J., Li, L., Chen, C., Huang, C., Huang, H., Feng, J., Wang, S., Wang, H., Zhang, G., Zhou, M., Cheng, P., Wu, M., Sheng, G., Fu, J., Hu, Y., Russell, A. G., and Wumaer, A.: Source apportionment of fine particulate matter during autumn haze episodes in Shanghai, China, J. Geophys. Res. Atmos., 119, 1903–1914, doi:10.1002/2013JD019630, 2014.

Wang, Y.X., Zhang, Q., Jiang, J., Zhou, W., Wang, B., He, K., Duan, F., Zhang, Q., Philip, S., and Xie, Y.: Enhanced sulfate formation during China's severe winter haze episode in January 2013 missing from current models, J. Geophys. Res. Atmos., 119, 10,425-10,440, doi:10.1002/2013JD021426, 2014.

Wang, Z., Liu, D., Wang, Y., and Shi, G.: Diurnal aerosol variations do affect daily averaged radiative forcing under heavy aerosol loading observed in Hefei, China, Atmos. Meas. Tech., 8, 2901–2907, doi:10.5194/amt-8-2901-2015, 2015.

Wang, Z.F., Li, J., Wang, Z., Yang, W., Tang, X., Ge, B., Yan, P., Zhu, L., Chen, X., Chen, H., Wand, W., Li, J., Liu, B., Wang, X., Zhao, Y., Lu, N., and Su, D.: Modeling study of regional severe hazes over mid-eastern China in January 2013 and its implications on pollution prevention and control, Sci. China Earth Sci., 57, 3–13, doi:10.1007/s11430-013-4793-0, 2014.

Wiedinmyer, C., Akagi, S. K., Yokelson, R. J., Emmons, L. K., Al-Saadi, J. A., Orlando, J. J., and Soja, A. J.: The Fire INventory from NCAR (FINN) – a high resolution global model to estimate the emissions from open burning, Geosci. Model Dev. Discuss., 3, 2439–2476, doi:10.5194/gmdd-3-2439-2010, 2010.

Woo J H, Baek J M, Kim J W, et al.: Development of a multi-resolution emission inventory and its impact on sulfur distribution for Northeast Asia, Water, air, and soil pollution, 148(1-4): 259-278, 2003.

WRAP (Western Regional Air Partnership): 2002 Fire Emission Inventory for the WRAP Region- Phase II, Project No. 178-6, available at: http://www.wrapair.org/forums/fejf/tasks/FEJFtask7PhaseII.html (last access: 02 January 2020), 22 July 2005.

Wu, L., Su, H., and Jiang, J. H.: Regional simulation of aerosol impacts on precipitation during the East Asian summer monsoon, J. Geophys. Res. Atmos., 118, 6454–6467, doi:10.1002/jgrd.50527, 2013.

Xie, Y., Zhao, B., Zhang, L., and Luo, R.: Spatiotemporal variations of $PM_{2.5}$ and PM_{10} concentrations between 31 Chinese cities and their relationships with SO_2, NO_2, CO and O_3, Particuology, 20, 141–149, doi:10.1016/j.partic.2015.01.003, 2015.

1237 Xu, W. Y., Zhao, C. S., Ran, L., Lin, W. L., Yan, P., & Xu, X. B.: SO_2 noontime-peak
1238 phenomenon in the North China Plain, Atmospheric Chemistry and Physics, 14,
1239 7757-7768, 2014.
1240 Xu, W., Sun, Y., Wang, Q., Zhao, J., Wang, J., Ge, X., Xie, C., Zhou, W., Du, W., Li, J.,
1241 Fu, P., Wang, Z., Worsnop, D. R., and Coe, H.: Changes in Aerosol Chemistry From
1242 2014 to 2016 in Winter in Beijing: Insights From High-Resolution Aerosol Mass
1243 Spectrometry, J. Geophys. Res. Atmos., 124, 1132–1147, doi:10.1029/2018JD029245,
1244 2019.
1245 Yang Y, Liao H, Lou S.: Increase in winter haze over eastern China in recent decades:
1246 Roles of variations in meteorological parameters and anthropogenic emissions,
1247 Journal of Geophysical Research: Atmospheres, 121,050-13,065, 2016.
1248 Yang, Y., Smith, S. J., Wang, H., Lou, S., and Rasch, P. J.: Impact of Anthropogenic
1249 Emission Injection Height Uncertainty on Global Sulfur Dioxide and Aerosol
1250 Distribution, J. Geophys. Res. Atmos., 124, 4812–4826, doi:10.1029/2018JD030001,
1251 2019.
1252 Ying, Z., Tie, X., and Li, G.: Sensitivity of ozone concentrations to diurnal variations of
1253 surface emissions in Mexico City: A WRF/Chem modeling study, Atmospheric
1254 Environment, 43, 851–859, doi:10.1016/j.atmosenv.2008.10.044, 2009.
1255 Zaveri, R. A. and Peters, L. K.: A new lumped structure photochemical mechanism for
1256 large-scale applications, J. Geophys. Res., 104, 30387–30415,
1257 doi:10.1029/1999JD900876, 1999.
1258 Zaveri, R. A., Easter, R. C., Fast, J. D., & Peters, L. K.: Model for simulating aerosol
1259 interactions and chemistry (MOSAIC), Journal of Geophysical Research:
1260 Atmospheres, 113, 2008.
1261 Zhang, B., Wang, Y., and Hao, J.: Simulating aerosol–radiation–cloud feedbacks on
1262 meteorology and air quality over eastern China under severe haze conditionsin winter,
1263 Atmos. Chem. Phys., 15, 2387–2404, doi:10.5194/acp-15-2387-2015, 2015.
1264 Zhang, H., Wang, Y., Hu, J., Ying, Q., and Hu, X.-M.: Relationships between
1265 meteorological parameters and criteria air pollutants in three megacities in China,
1266 Environmental research, 140, 242–254, doi:10.1016/j.envres.2015.04.004, 2015.
1267 Zhang, L., Liao, H., and Li, J.: Impacts of Asian summer monsoon on seasonal and
1268 interannual variations of aerosols over eastern China, J. Geophys. Res., 115, D10307,
1269 doi:10.1029/2009JD012299, 2010.

Zhang, L., Wang, T., Lv, M., and Zhang, Q.: On the severe haze in Beijing during January 2013: Unraveling the effects of meteorological anomalies with WRF-Chem, Atmospheric Environment, 104, 11–21, doi:10.1016/j.atmosenv.2015.01.001, 2015.

Zhang, R., Li, G., Fan, J., Wu, D. L., and Molina, M. J.: Intensification of Pacific storm track linked to Asian pollution, Proceedings of the National Academy of Sciences of the United States of America, 104, 5295–5299, doi:10.1073/pnas.0700618104, 2007.

Zhang, Y., Zhang, X., Wang, L., Zhang, Q., Duan, F., and He, K.: Application of WRF/Chem over East Asia: Part I. Model evaluation and intercomparison with MM5/CMAQ, Atmospheric Environment, 124, 285–300, doi:10.1016/j.atmosenv.2015.07.022, 2016.

Zhang, Y.-L. and Cao, F.: Fine particulate matter ($PM_{2.5}$) in China at a city level, Scientific reports, 5, 14884, doi:10.1038/srep14884, 2015.

Zhao C, Liu X, Leung L R.: Impact of the Desert dust on the summer monsoon system over Southwestern North America, Atmospheric Chemistry and Physics, 12, 3717-3731, 2012.

Zhao, B., Liou, K.-N., Gu, Y., Li, Q., Jiang, J. H., Su, H., He, C., Tseng, H.-L. R., Wang, S., Liu, R., Qi, L., Lee, W.-L., and Hao, J.: Enhanced $PM_{2.5}$ pollution in China due to aerosol-cloud interactions, Scientific reports, 7, 4453, doi:10.1038/s41598-017-04096-8, 2017.

Zhao, C., Chen, S., Leung, L. R., Qian, Y., Kok, J., Zaveri, R., and Huang, J.: Uncertainty in modeling dust mass balance and radiative forcing from size parameterization, Atmospheric Chemistry and Physics, 13, 10733-10753, 2013a.

Zhao, C., Hu, Z., Qian, Y., Leung, L. R., Huang, J., Huang, M., Jin, J., Flanner, M., Zhang, R., Wang, H., Yan, H., Lu, Z., and Streets, D. G.: Simulating black carbon and dust and their radiative forcing in seasonal snow: a case study over North China with field campaign measurements, Atmospheric Chemistry and Physics, 14, 11475-11491, 2014.

Zhao, C., Huang, M., Fast, J. D., Berg, L. K., Qian, Y., Guenther, A., ... & Pfister, G.: Sensitivity of biogenic volatile organic compounds to land surface parameterizations and vegetation distributions in California, Geosci. Model Dev, 9, 1959-1976, 2016.

Zhao, C., Liu, X., Leung, L. R., and Hagos, S.: Radiative impact of mineral dust on monsoon precipitation variability over West Africa, Atmospheric Chemistry and Physics, 11, 1879-1893, 2011.

Zhao, C., Liu, X., Leung, L. R., Johnson, B., McFarlane, S. A., Gustafson, W. I., Fast, J. D., and Easter, R.: The spatial distribution of mineral dust and its shortwave radiative forcing over North Africa: modeling sensitivities to dust emissions and aerosol size treatments, Atmospheric Chemistry and Physics, 10, 8821-8838, 2010.

Zhao, C., Ruby Leung, L., Easter, R., Hand, J., and Avise, J.: Characterization of speciated aerosol direct radiative forcing over California, J. Geophys. Res. Atmos., 118, 2372–2388, doi:10.1029/2012JD018364, 2013b.

Zhao, S., Yu, Y., Yin, D., He, J., Liu, N., Qu, J., and Xiao, J.: Annual and diurnal variations of gaseous and particulate pollutants in 31 provincial capital cities based on in situ air quality monitoring data from China National Environmental Monitoring Center, Environment international, 86, 92–106, doi:10.1016/j.envint.2015.11.003, 2016.

Zhong M, Saikawa E, Liu Y, et al. Air quality modeling with WRF-Chem v3. 5 in East Asia: sensitivity to emissions and evaluation of simulated air quality[J]. Geoscientific Model Development, 2016, 9(3).

Zhou, G., Xu, J., Xie, Y., Chang, L., Gao, W., Gu, Y., and Zhou, J.: Numerical air quality forecasting over eastern China: An operational application of WRF-Chem, Atmospheric Environment, 153, 94–108, doi:10.1016/j.atmosenv.2017.01.020, 2017.

Zhou, G., Yang, F., Geng, F., Xu, J., Yang, X., Tie, X.: Measuring and modeling aerosol: relationship with haze events in Shanghai, China, Aerosol and air quality research, 14, 783-792, 2014.

Table 1 Numerical experiments conducted in this study.

Name	PBL scheme	Vertical structure	PBL mixing coefficient (m^2/s)	Emission diurnal cycle	Emission injection height
CTL1	MYNN	layer1	Minimum=0.1	Yes	Yes
CTL2	MYNN	layer2	Minimum=0.1	Yes	Yes
CTL3	YSU	layer2	Minimum=0.1	Yes	Yes
EXP1	MYNN	layer1	Minimum = 5.0	Yes	Yes
EXP2	MYNN	layer2	Minimum = 5.0	Yes	Yes
EXP1_E1	MYNN	layer1	Minimum = 5.0	No	Yes
EXP1_E2	MYNN	layer1	Minimum = 5.0	Yes	No

Table 2 Vertical distributions of power plant emissions: percentage of each species allocated to the height of the vertical layers in the WRF-Chem model.

Species	Height of Emission Layers (m)				
	0-76	**76-153**	**153-308**	**308-547**	**547-871**
SO_2	5%	30%	35%	25%	5%
NO_x	5%	40%	25%	25%	5%
CO	5%	70%	20%	5%	0%
NH_3	5%	75%	15%	5%	0%
NMVOC	5%	85%	10%	0%	0%
$PM_{2.5}$	5%	45%	25%	20%	5%
PM_{10}	5%	55%	20%	15%	5%
OC	5%	70%	15%	10%	0%
BC	5%	65%	20%	10%	0%

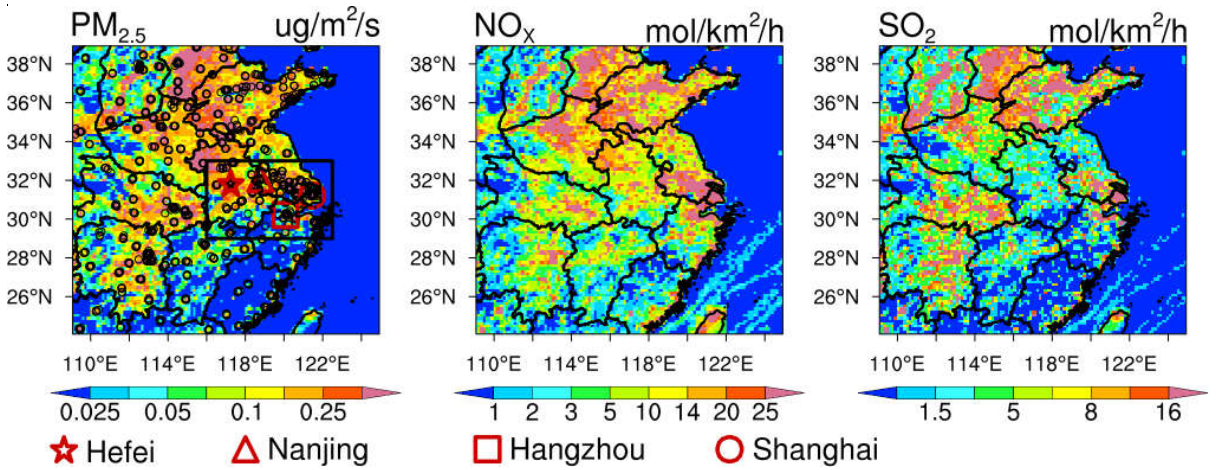

Figure 1a. Emissions of SO_2, NO_2, $PM_{2.5}$ from the MEIC China inventory over the simulation domain (109.0° E~124.9° E, 24.0° N~38.9° N) with black boxes showing the analyzed domain (116.0° E~122.5° E, 29.0° N~33.0° N), overlaid with observational sites and four cities as the Center (Shanghai, 121.45°E and 31.21°N) and sub-Center (Nanjing, 118.78°E and 32.06°N; Hefei, 117.25°E and 31.85°N; Hangzhou, 120.08°E and 30.21°N) of the YRD city cluster.

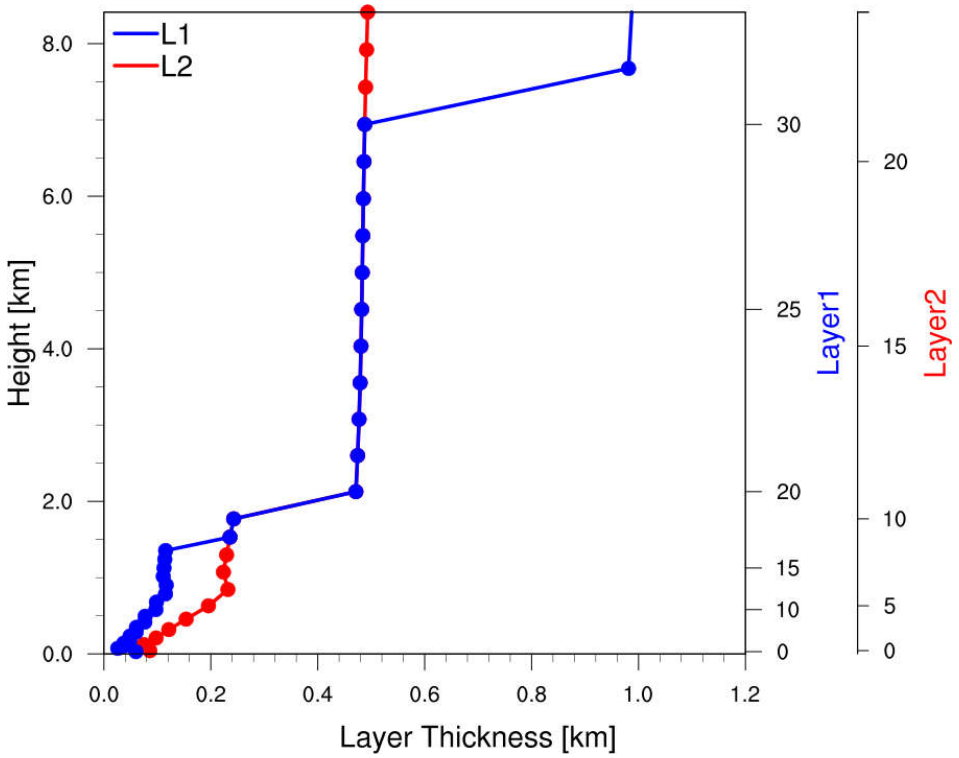

Figure 1b. Vertical profiles of the layer thickness from L1 and L2 layer configuration.

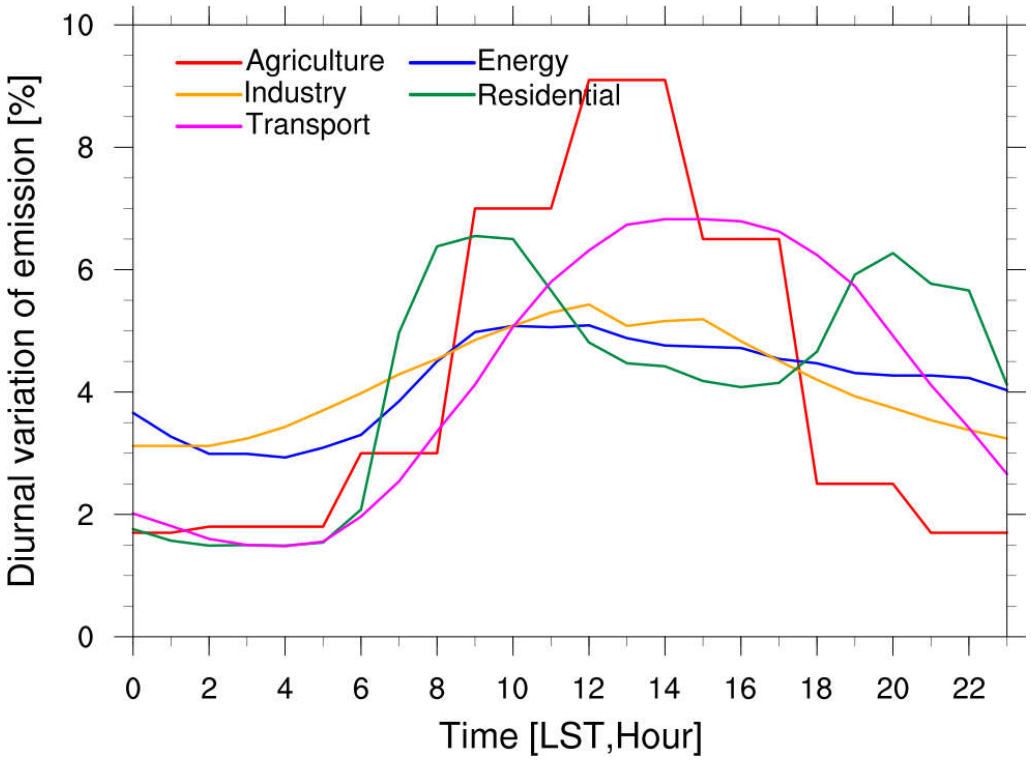

Figure 1c. Diurnal profiles of emissions from five individual sectors (agriculture, industry, transport, energy, and residential).

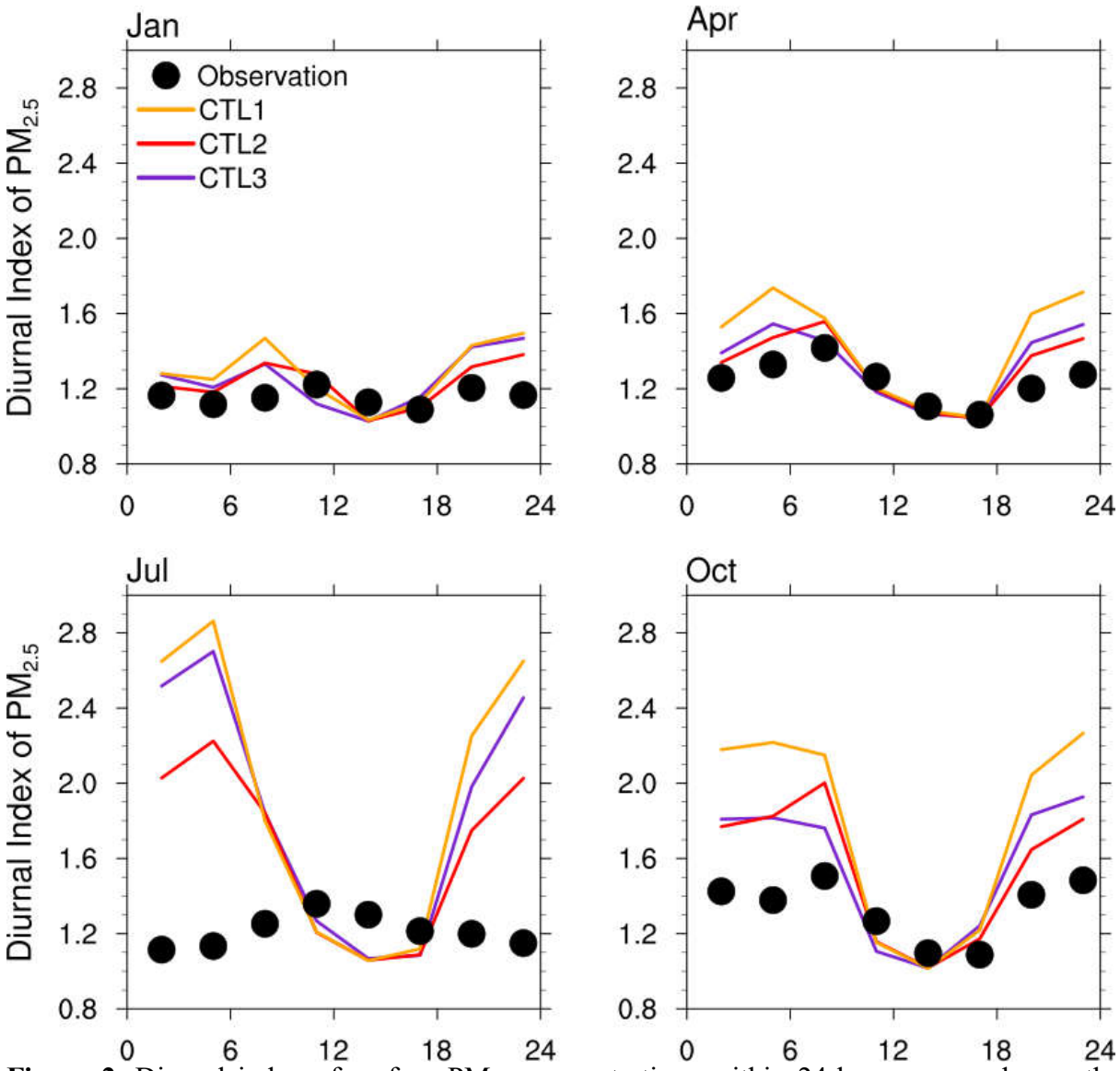

Figure 2. Diurnal index of surface $PM_{2.5}$ concentrations within 24-hour averaged over the YRD region of East China (within the black box of Fig. 1a) for January, April, July, and October of 2018 from the experiments CTL1, CTL2, CTL3, and observations. Both the simulated results and observations are sampled at the model output frequency, i.e., 3-hourly.

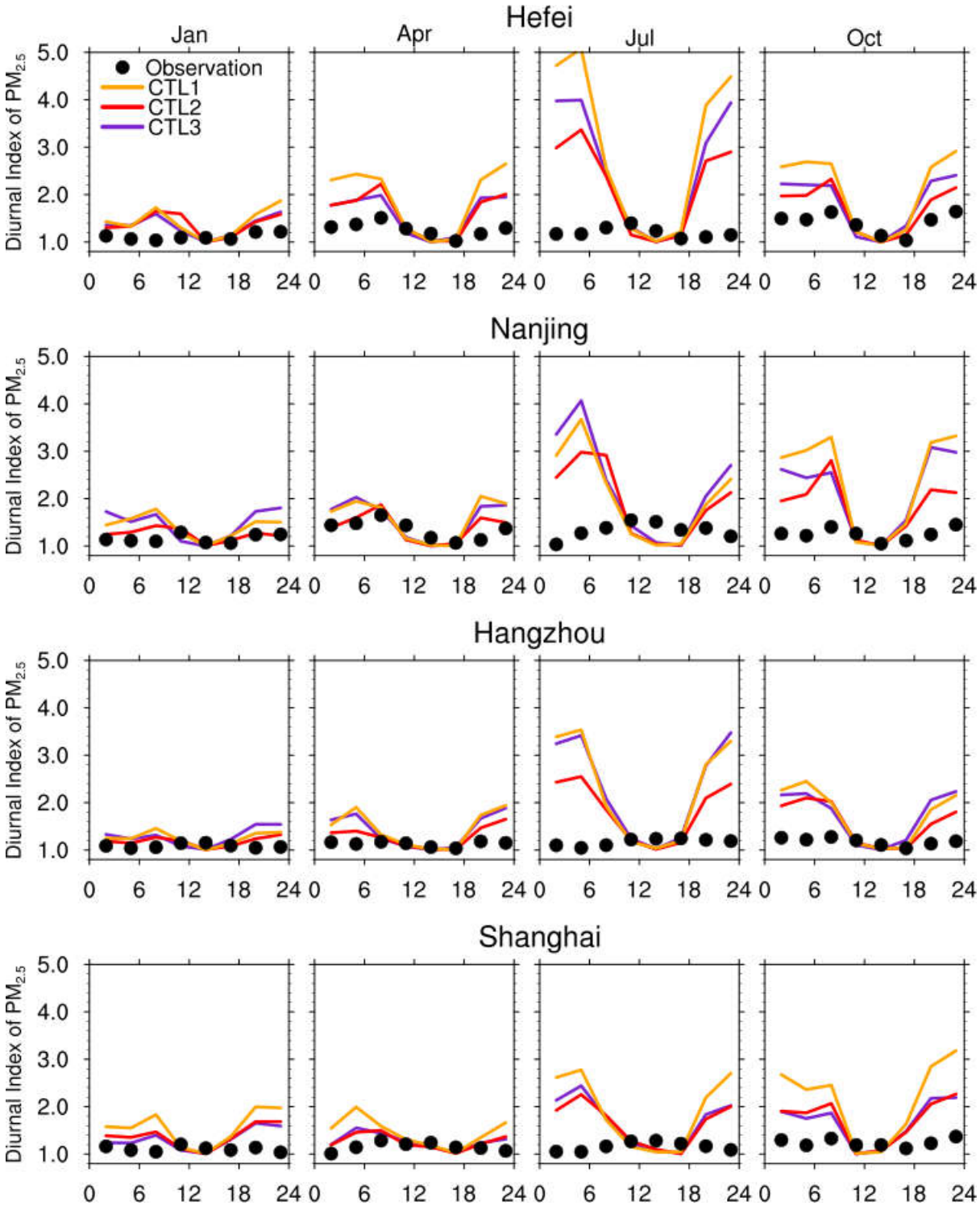

Figure 3. Diurnal index of surface $PM_{2.5}$ concentrations within 24-hour averaged over four cities (Hefei, Nanjing, Hangzhou, Shanghai) for January, April, July, and October of 2018 from the experiments CTL1, CTL2, CTL3, and observations.

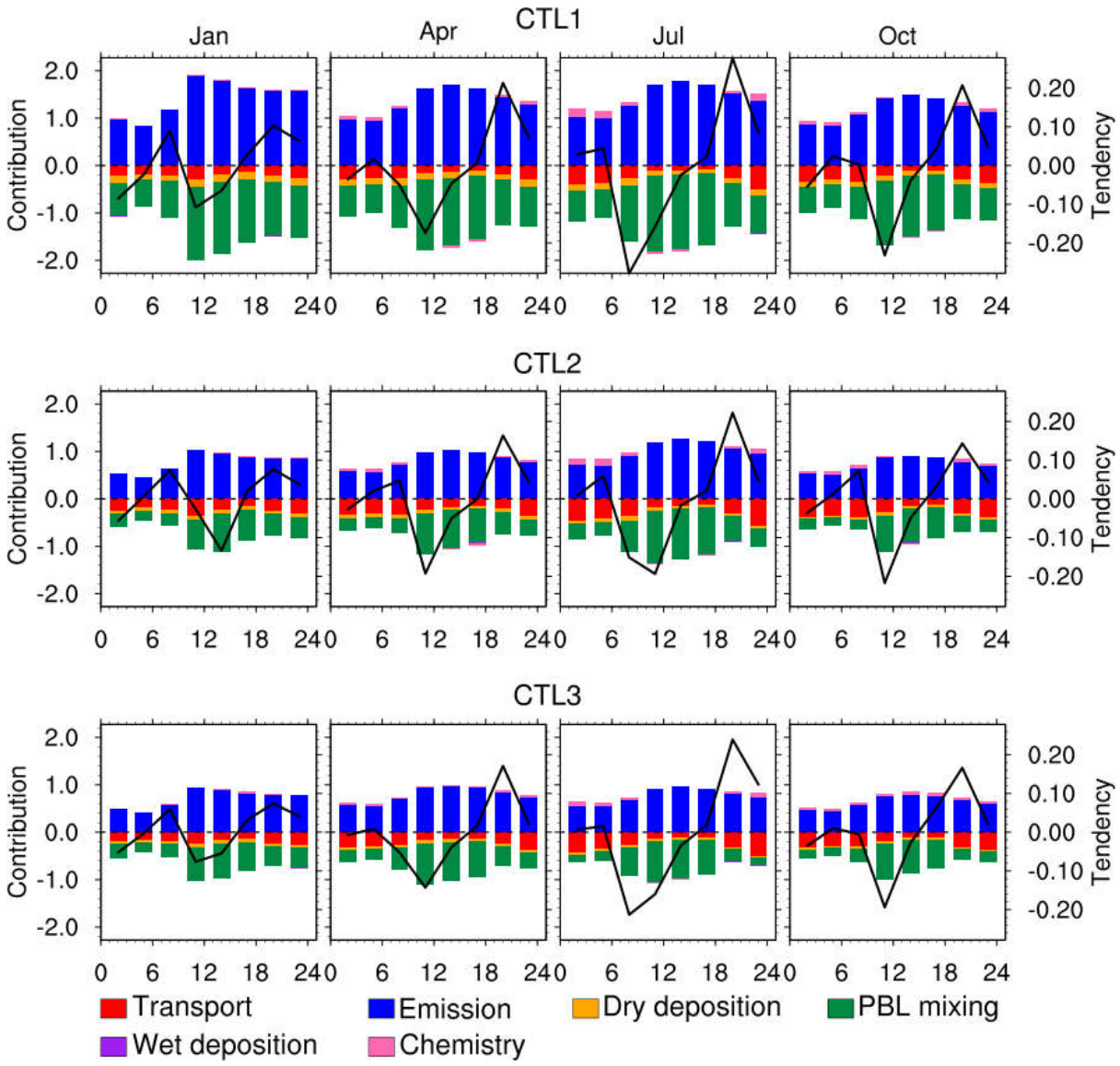

Figure 4. Relative contribution (normalized by monthly mean surface $PM_{2.5}$ concentrations for each month) to surface $PM_{2.5}$ concentrations every 3-hour from individual process (transport, emission, dry and wet deposition, PBL mixing, chemical production/loss) averaged over Hefei for January, April, July, and October of 2018 from the experiments CTL1, CTL2, and CTL3. The 3-hourly relative tendency of surface $PM_{2.5}$ concentrations is also shown as the black line.

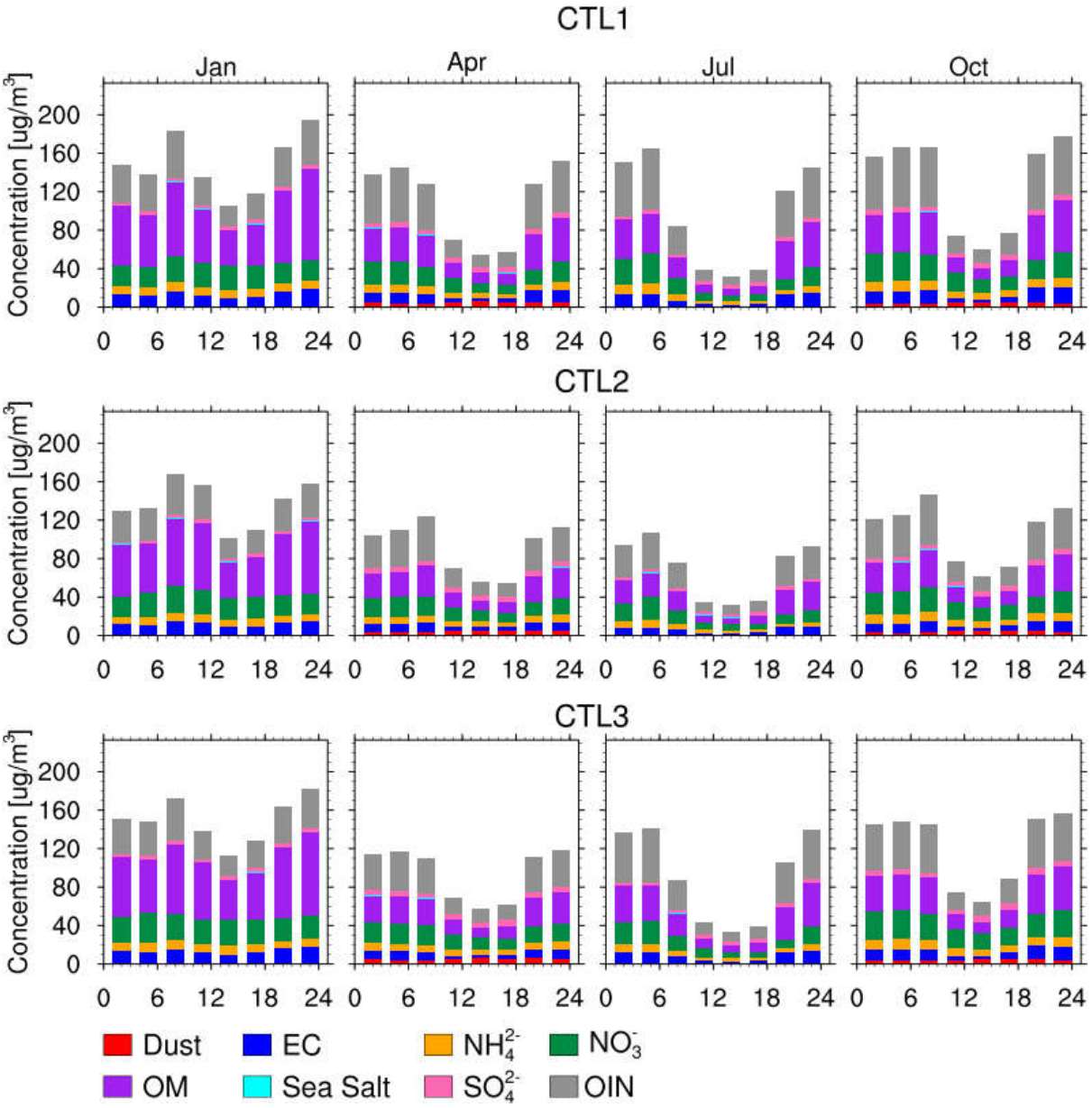

Figure 5. Diurnal variation of surface concentrations of each $PM_{2.5}$ composition (Dust, OM, EC, Sea Salt, NH_4^{2-}, SO_4^{2-}, NO_3^-, and other inorganics) averaged over Hefei for January, April, July, and October of 2018 from the experiments CTL1, CTL2, and CTL3.

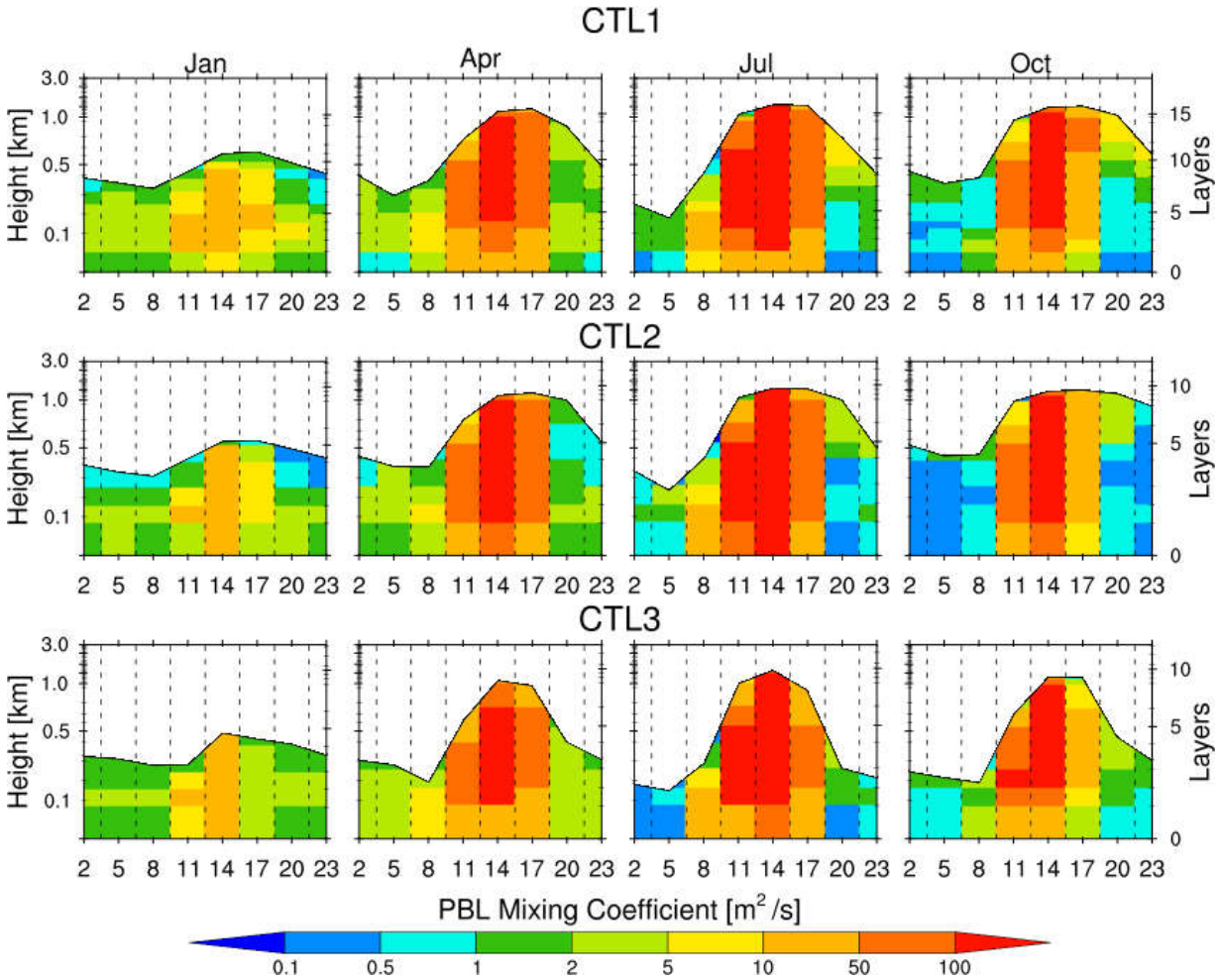

Figure 6. Diurnal variation of PBLH and PBL mixing coefficient below PBLH averaged over Hefei for January, April, July, and October of 2018 from the experiments CTL1, CTL2, and CTL3.

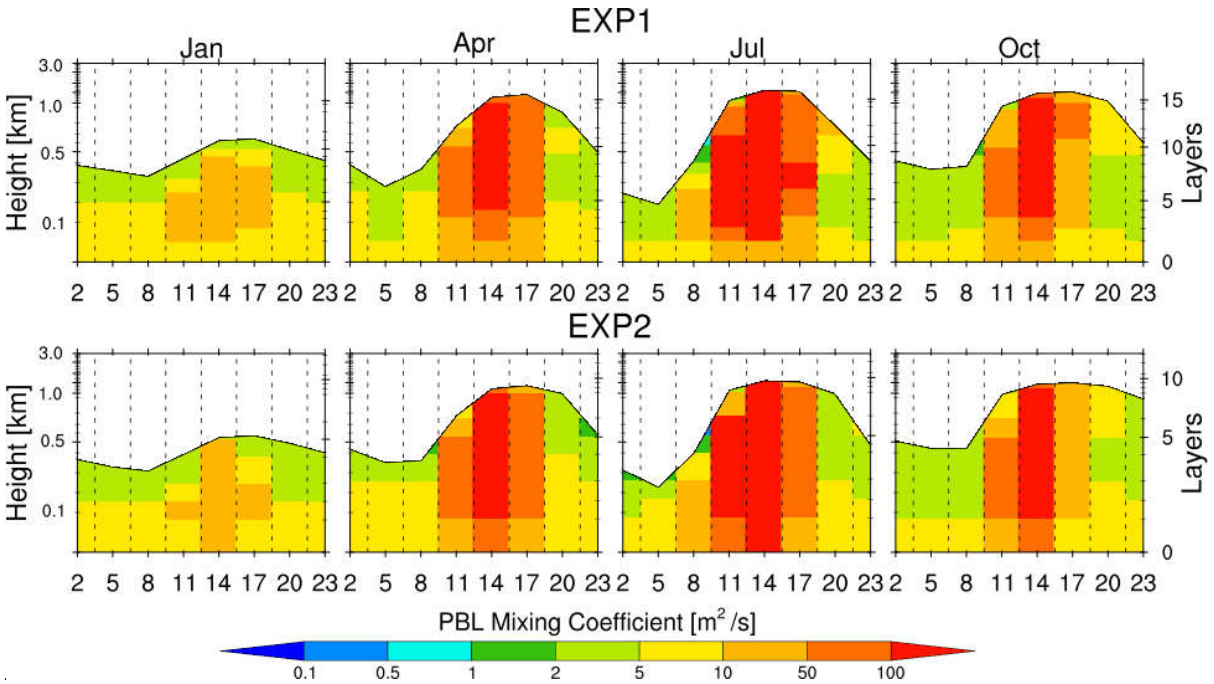

Figure 7. Diurnal variation of PBLH and PBL mixing coefficient below PBLH averaged over Hefei for January, April, July, and October of 2018 from the experiments EXP1 and EXP2.

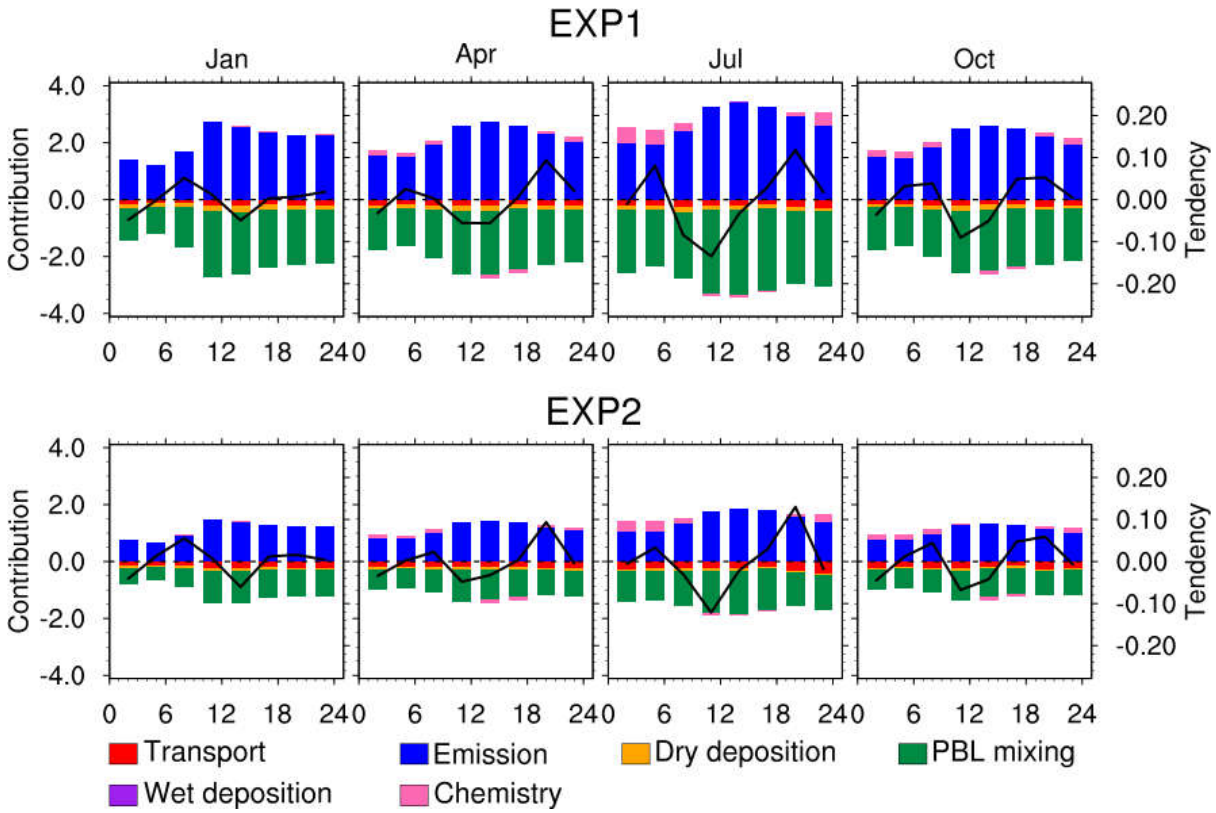

Figure 8. Relative contribution (normalized by monthly mean surface $PM_{2.5}$ concentrations for each month) to surface $PM_{2.5}$ concentrations every 3-hour from individual process (transport, emission, dry and wet deposition, PBL mixing, chemical production/loss) averaged over Hefei for January, April, July, and October of 2018 from the experiments EXP1 and EXP2. The 3-hourly relative tendency of surface $PM_{2.5}$ concentrations is also shown as the black line.

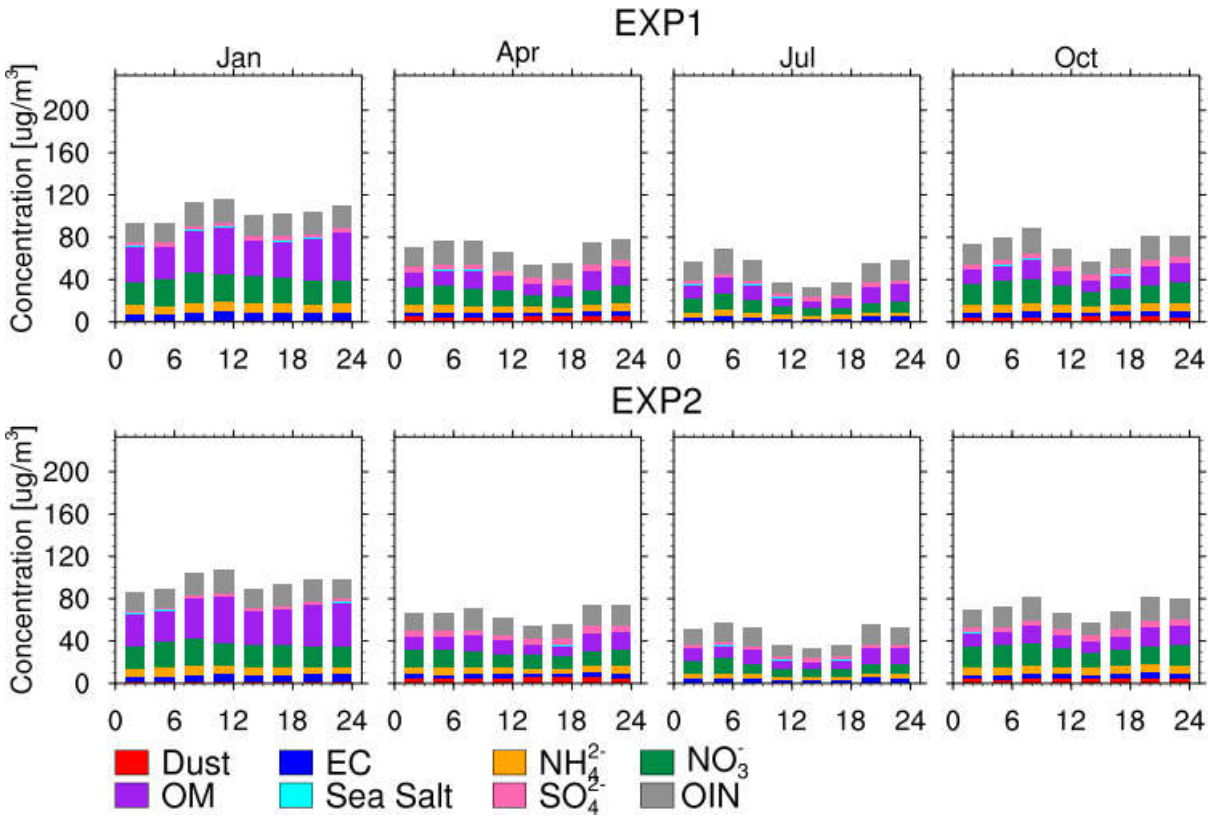

Figure 9. Diurnal cycle of surface $PM_{2.5}$ composition concentrations (Dust, OM, EC, Sea Salt, NH_4^{2-}, SO_4^{2-}, NO_3^-, and other inorganics) averaged over Hefei for January, April, July, and October of 2018 from the experiments EXP1 and EXP2.

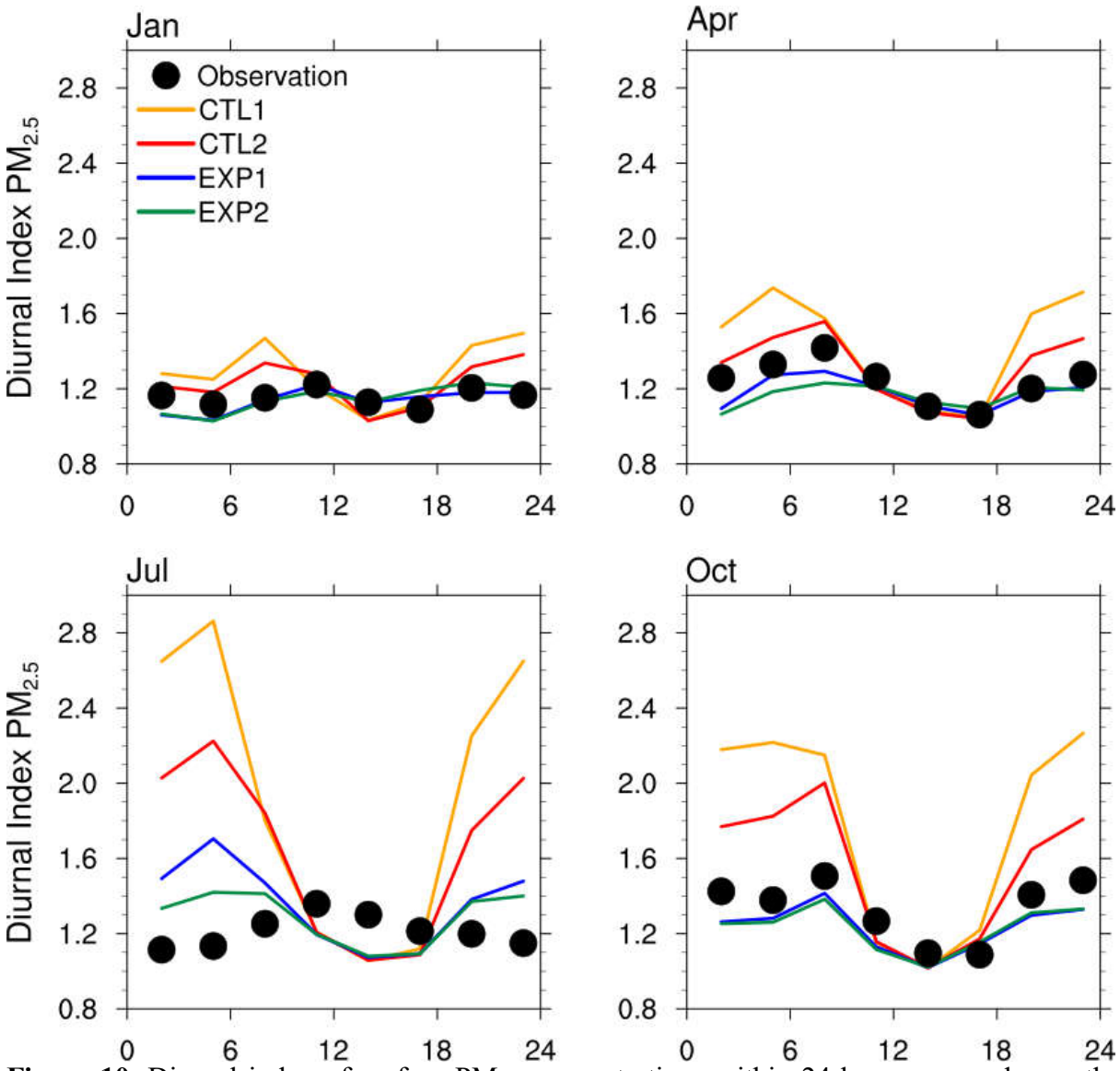

Figure 10. Diurnal index of surface $PM_{2.5}$ concentrations within 24-hour averaged over the YRD region of East China (within black box of Fig. 1a) for January, April, July, and October of 2018 from the experiments CTL1, CTL2, EXP1, EXP2, and observations. Both the simulated results and observations are sampled at the model output frequency, i.e., 3-hourly.

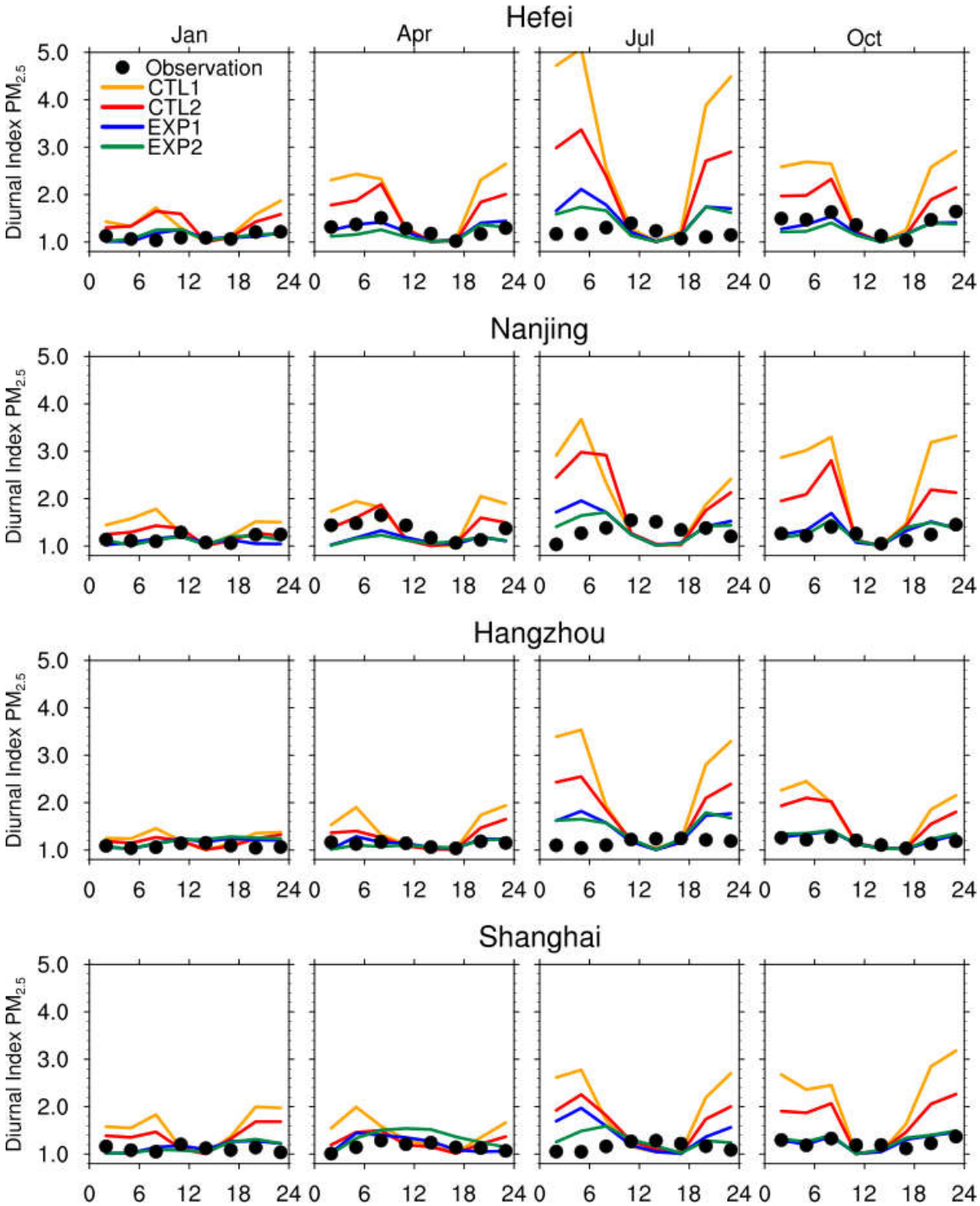

Figure 11. Diurnal index of surface $PM_{2.5}$ concentrations within 24-hour averaged over four cities (Hefei, Nanjing, Hangzhou, Shanghai) for January, April, July, and October of 2018 from the experiments CTL1, CTL2, EXP1, EXP2, and observations.

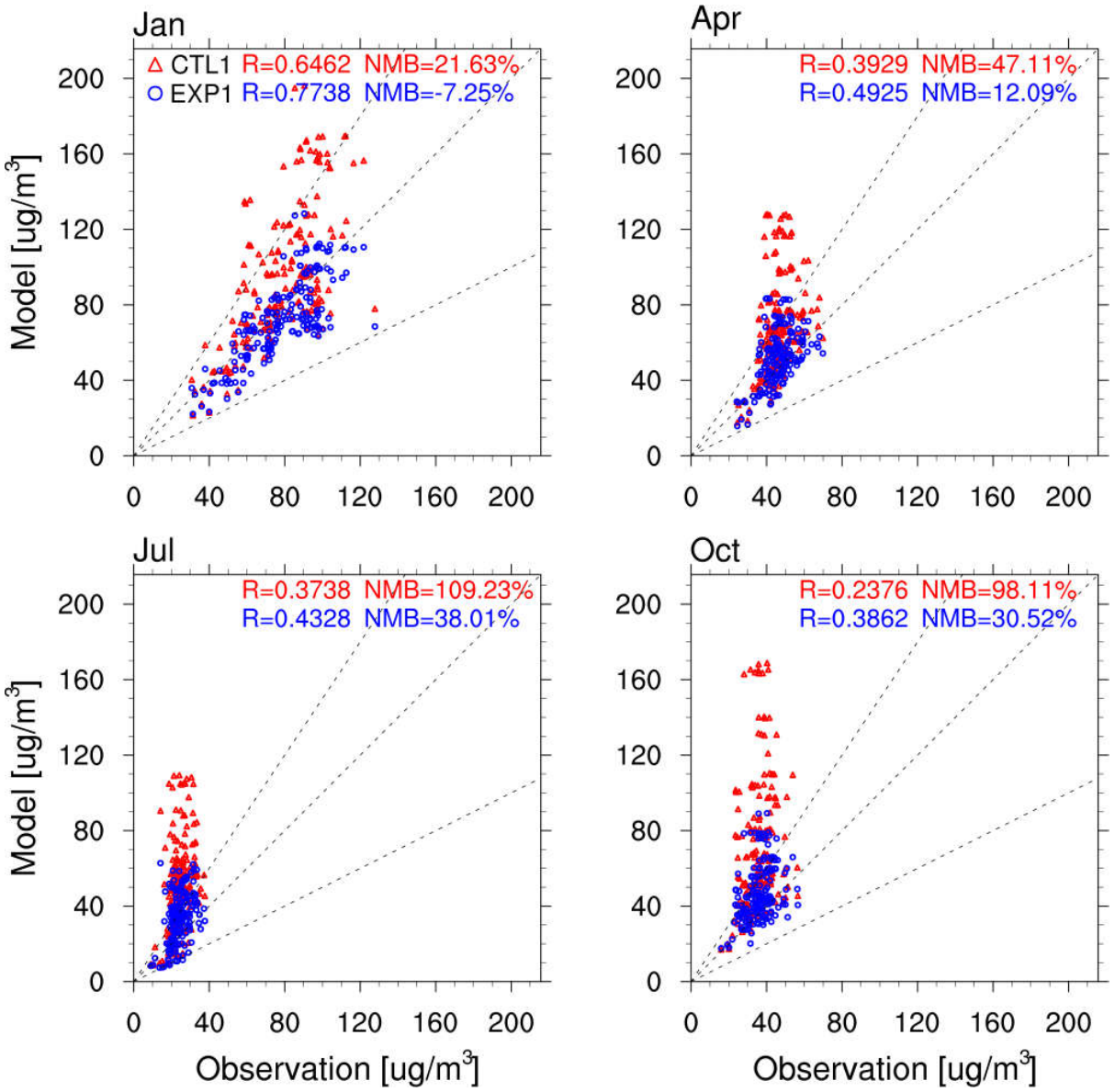

Figure 12. Comparison of monthly mean surface $PM_{2.5}$ concentrations between the observations and the simulations from the experiments CTL1 and EXP1 at each observation site over the YRD region of East China (as shown in Fig. 1a within the black box) for January, April, July, and October of 2018. The dashed lines represent -50%, 0, 50% of the NMB of simulation.

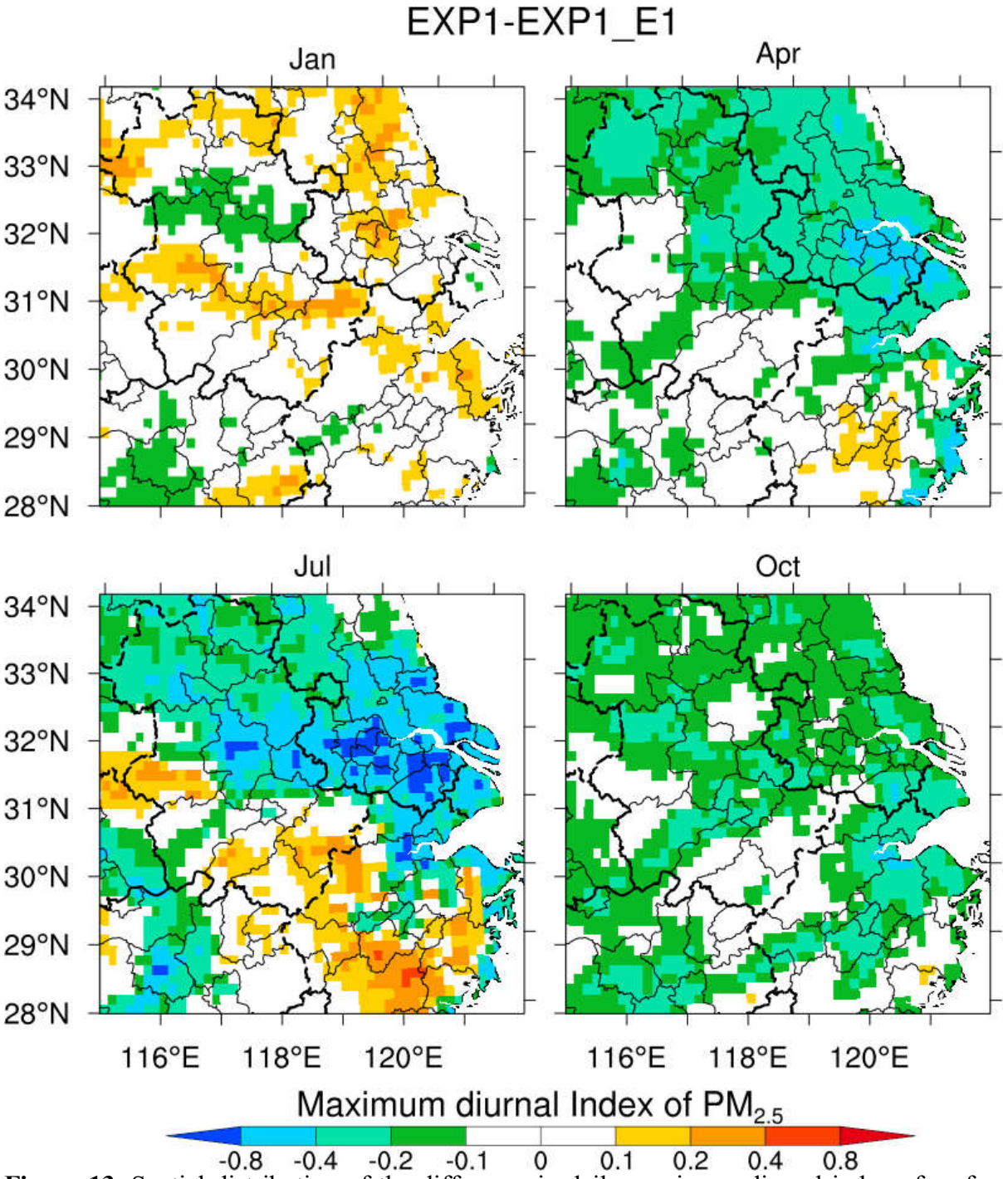

Figure 13. Spatial distribution of the difference in daily maximum diurnal index of surface $PM_{2.5}$ concentrations between the experiments EXP1 and EXP1_E1 over East China in January, April, July, and October of 2018.

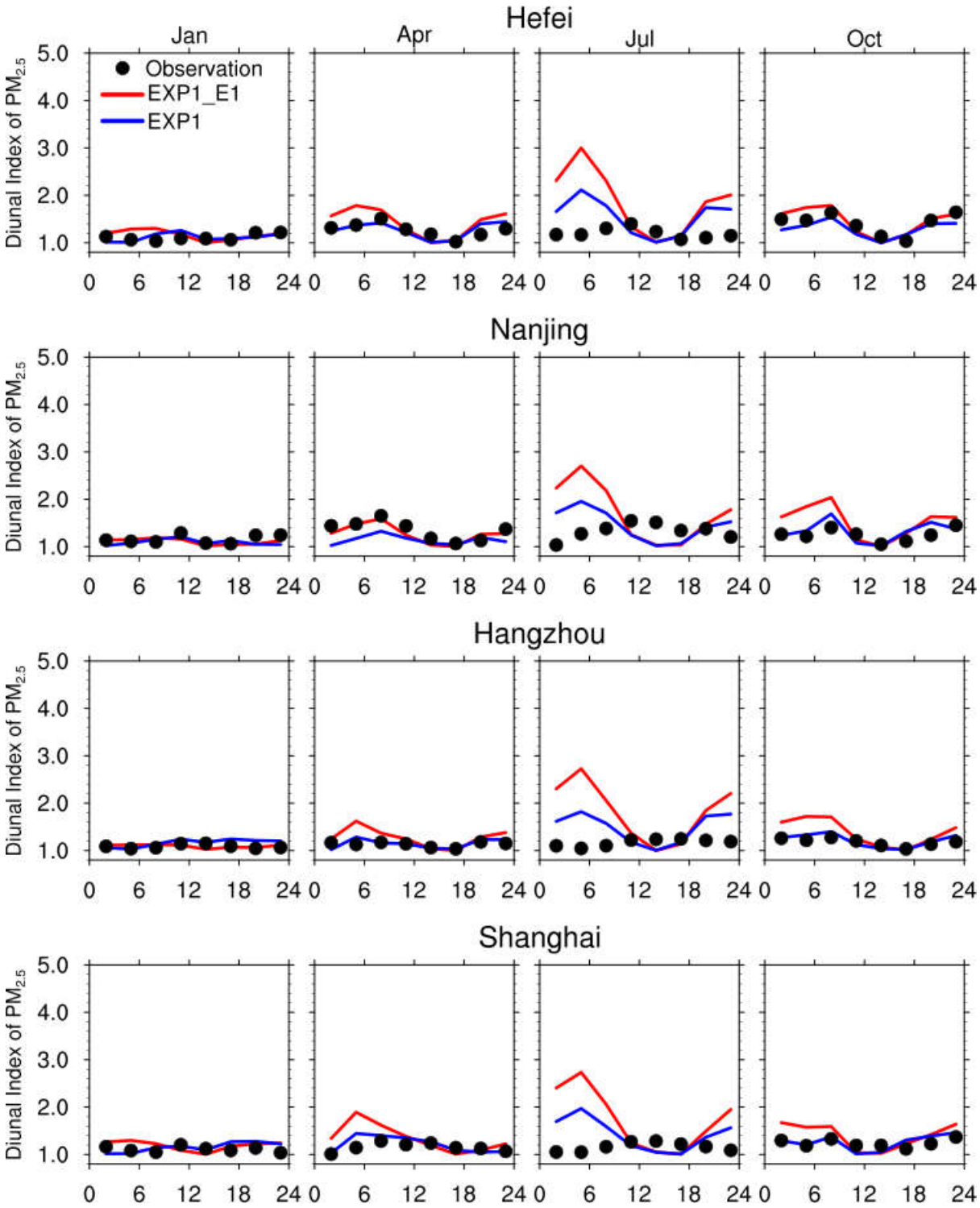

Figure 14. Diurnal index of surface $PM_{2.5}$ concentrations within 24-hour averaged over four cities (Hefei, Nanjing, Hangzhou, Shanghai) for January, April, July, and October of 2018 from the experiments EXP1_E1, EXP1, and observations.

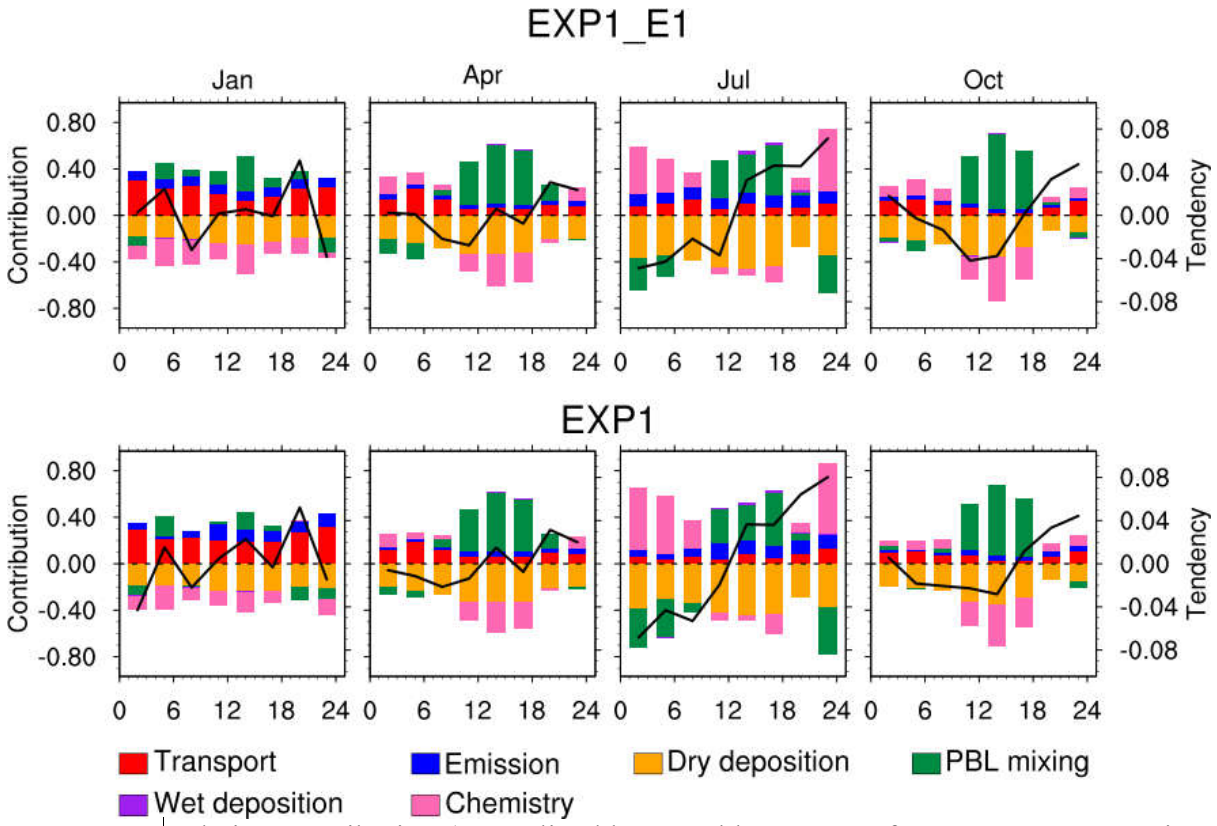

Figure 15. Relative contribution (normalized by monthly mean surface $PM_{2.5}$ concentrations for each month) to surface $PM_{2.5}$ concentrations every 3-hour from individual process (transport, emission, dry and wet deposition, PBL mixing, chemical production/loss) averaged over south Anhui for January, April, July, and October of 2018 from the experiments EXP1_E1 and EXP1. The 3-hourly relative tendency of surface $PM_{2.5}$ concentrations is also shown as the black line.

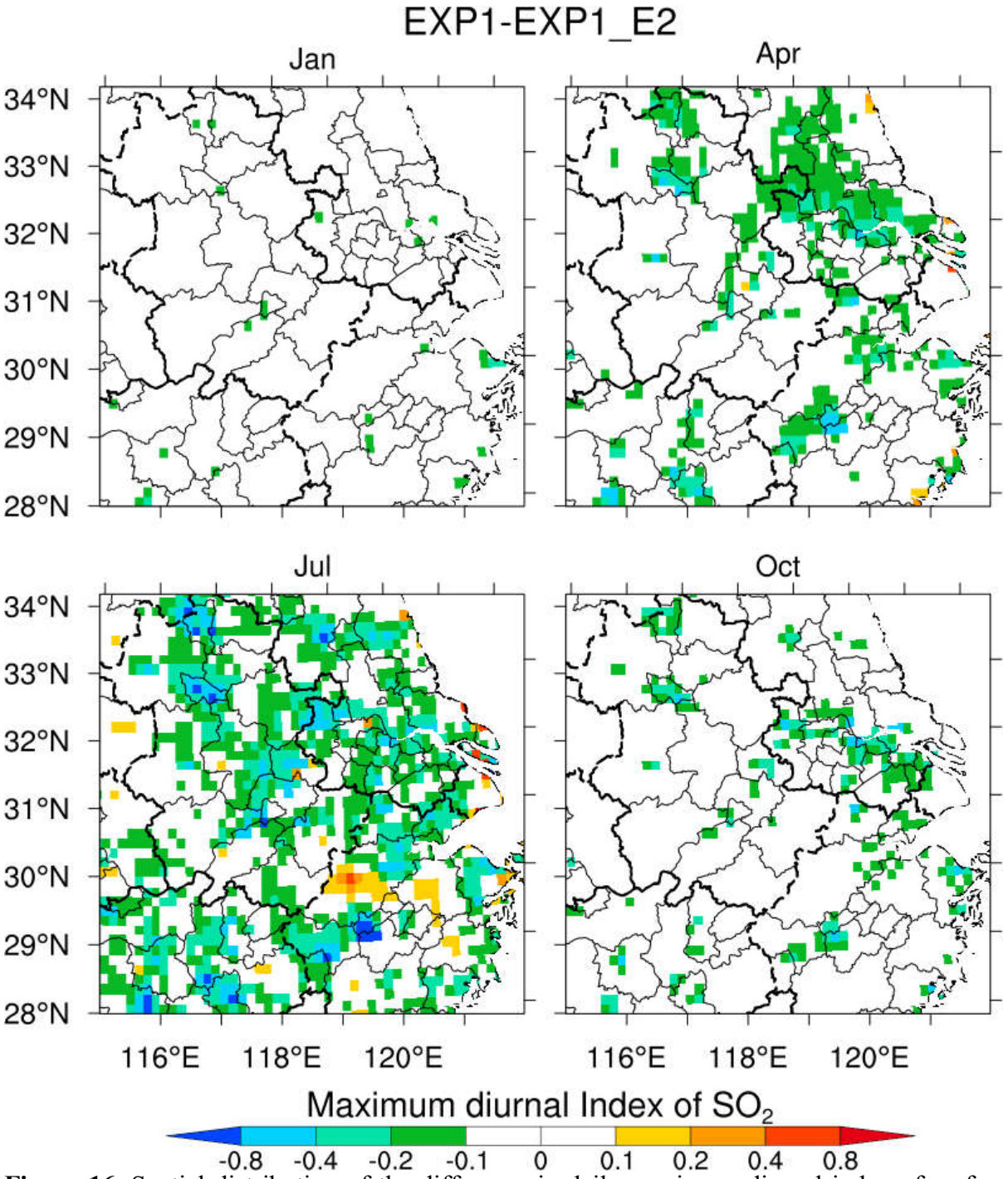

Figure 16. Spatial distribution of the difference in daily maximum diurnal index of surface SO_2 concentrations between the experiments EXP1_E2 and EXP1 over East China in January, April, July, and October of 2018.